T.C.

KIRIKKALE UNIVERSITY

GRADUATE SCHOOL OF NATURAL AND APPLIED SCIENCES

NUMERICAL INVESTIGATION OF THE EFFECTS OF BAFFLE GEOMETRY AND NUMBER ON THE FLOW STRUCTURE AND ACOUSTICS IN A GUN SUPPRESSOR

EZEDIN AYALIEW YIMAM

DEPARTMENT OF MECHANICAL ENGINEERING

MASTER'S THESIS

SUPERVISOR

Assist. Prof. Dr. Tolga DEMIRCAN

KIRIKKALE 2022

The thesis study entitled NUMERICAL INVESTIGATION OF THE EFFECTS OF BAFFLE GEOMETRY AND NUMBER ON THE FLOW STRUCTURE AND ACOUSTICS IN A GUN SUPPRESSOR, prepared by EZEDIN AYALIEW YIAMA" has been unanimously accepted by the following jury as a MASTERS THESIS in Kırıkkale University, Institute of Science and Technology, Department of Mechanical Engineering.

Advisor: Assist. Prof. Dr. Tolga DEMIRCAN Signature

Mechanical Engineering Department,

Kırıkkale University

I certify that this thesis is a MastersThesis in terms of scope and quality.

Chairman: Prof. Dr. Yahya DOĞU Signature

Mechanical Engineering Department,

Kırıkkale University

I certify that this thesis is a MastersThesis in terms of scope and quality.

Member: Prof. Dr. Sinan Çalışkan
Signature

Mechanical Engineering Department,

Hitit University

I certify that this thesis is a MastersThesis in terms of scope and quality.

Thesis Defense Date: 30/09/2022

I certify that this thesis, accepted by the jury, fulfills the requirements for a Master's Thesis.

Prof. Dr. Recep ÇALIN

Director of the Graduate School of Natural and Applied Sciences

ABSTRACT

NUMERICAL INVESTIGATION OF THE EFFECTS OF BAFFLE GEOMETRY AND NUMBER ON THE FLOW STRUCTURE AND ACOUSTICS IN A GUN SUPPRESSOR

Kırıkkale University

Graduate School of Natural and Applied Sciences

Department of Mechanical Engineering, Master's Thesis

Supervisor: Assist. Prof. Dr. Tolga DEMIRCAN

September 2022, 93 pages

Supersonic propellant gas is discharged from the barrel during the gunfire. Near the muzzle, the supersonic speed creates an unstable flow with high temperature, pressure, and velocity. This flow field generates a loud noise that has a lot of adverse effects on humans and the environment, so analyzing and attenuating this noise is essential.

This work aimed to examine propellant flow within and outside the suppressor using computational fluid dynamics (CFD). It also studied the suppressor effect on sound attenuation using the computational aeroacoustics (CAA) model. The fluid flow study was simulated using a pressure-based 3D axisymmetric and transient kω-SST turbulence model. The Ffowcs-Williams and Hawkins equations (FW-H) were utilized for the aeroacoustics simulation. The second-order implicit time approach for transient simulation and the second-order upwind scheme for spatial discretization was used.

Validation was done by comparing the numerical and experimental results of overpressure reduction and average sound amplitude attenuation. According to the comparison, this numerical method was found to be compatible. The effects of critical parameters, such as the suppressor's baffle shape, the baffling number, and suppressor volume, were studied without considering the projectile effect. Finally, the overpressure and acoustics results were compared with and without the suppressor.

The maximum overpressure reduction straight and L-shaped baffle suppressors were 75.45% and 79.75%, respectively, achieved with five baffles. The overpressure reduction of suppressors with five conical baffles was 79.55% and for suppressors with three Y-shaped baffles was 78.33%. The percentage drop in overpressure for the suppressor with one, three, and five curved baffles were 76.01%, 78.79%, and 81.3%, respectively, compared to the initial inlet pressure. The curved suppressor performed better than the other silencers examined in this study; further analysis was done for this silencer.

The maximum exit pressure for a suppressor with five curved baffles was 3.748 Mpa. However, when the diameter suppressor increased by 1/6, the maximum exit pressure was reduced to 3.4961Mpa. When the length increased by 1/6, the maximum pressure became 3.3636Mpa. Lastly, when the diameter and length were increased by 1/6, the maximum exit pressure became 3.177Mpa.

For unsuppressed conditions, 169.498 dB of SPL was recorded. When using a suppressor without a baffle, this value was reduced to 162.134 dB. For the suppressor with one, three, and five curved baffles, the SPL value was 160.234 dB, 159.437 dB, and 158.117 dB, respectively. For a suppressor with five curved baffles, when the diameter was increased by 1/6, the SPL attenuation increased to 16.515 dB and became 152.983 dB. When the length was increased by 1/6, the attenuation was 17.541 dB, and the SPLvalue became 150.956 dB. Lastly, when the suppressor diameter and length increased 1/6, The suppressor achieved a 20.835 dB (12.29 %) sound pressure level attenuation with 16.823 MPa (84.115 %) overpressure and 484.86 K or 32.32% temperature reduction.

Generally, This study shows that the suppressor's efficiency is directly proportional to its size, shape, and number of baffles. The attenuation increased with the increase in the suppressor's internal volume and the baffles' number and complexity.

Keywords: Flow noise, kω-SST turbulence model, Acoustic attenuation, Overpressure reduction, suppressor, Ffowcs Williams-Hawkings acoustic theory.

ÖZET

BİR SİLAH SUSTURUCUSUNDA PERDE GEOMETRİSİ VE SAYISININ AKIŞ YAPISI VE AKUSTİK ÜZERİNDEKİ ETKİLERİNİN SAYISAL İNCELENMESİ

Kırıkkale Üniversitesi

Fen Bilimleri Enstitüsü

Makine Mühendisliği Anabilim Dalı, Yüksek Lisans Tezi

Danışman: Dr. Öğretim Üyesi. Tolga DEMIRCAN

Eylül 2022, 93 Sayfa

Bir silahta ateşleme sırasında oluşan süpersonik hıza sahip itici gaz, yüksek basınç ve yüksek sıcaklığa ulaşarak namludan dış ortama doğru çıkış yapmaktadır. Bu namludan dış ortama aktarılan süpersonik hızlardaki gaz akışı nedeniyle, dış ortamda namlunun çıkışına yakın bölgelerde yüksek sıcaklık, yüksek hız ve yüksek basınçlara sahip dengesiz yapıda bir akış bölgesi oluşmaktadır. Oluşan bu akış bölgesi, ortamda bulunan insanlar ve çevre üzerinde birçok olumsuz etkiye sebep olabilen yüksek bir gürültünün oluşmasına neden olabilmektedir. Bundan dolayı, oluşan bu yüksek miktardaki gürültünün insan sağlığı ve çevre için güvenli olan seviyelere indirilmesi büyük önem arz etmektedir. Dolayısıyla bir silahın ateşlenmesi sırasında gerçekleşen ve gürültü oluşmasına sebebiyet veren tüm etkenlerin bir arada analiz edilmesi ve optimum susturucu geometrisi ve çalışma parametrelerinin belirlenmesi, oluşan gürültü seviyesinin azaltılabilmesi için çok önemlidir.

Bundan dolayı bu çalışmada, bir silah susturucusunun içinde ve susturucu çıkışına yakın bölgelerde dış ortamda gerçekleşen itici gaz akışı hesaplamalı akışkanlar dinamiği (HAD) yardımı ile incelenmiştir. Bu inceleme sırasında hem susturucu içindeki bölgeler için, hem de susturucudan çıkışta susturucuya yakın olan dış ortam bölgeleri için akışın sıcaklık, basınç, hız ve yoğunluk dağılımları elde edilerek irdelemeler yapılmıştır. Ayrıca hesaplamalı aeroakustik (HAA) modelini kullanarak, akustik incelemelerde bulunulmuş, susturucu geometrisinin ve çalışma parametrelerinin oluşan ses seviyesinin azaltılması üzerindeki susturucu etkileri de incelenmiştir.

Yapılan sayısal analizler sırasında, incelenen akış geometrisi üç boyutlu ve eksenel simetrik olarak oluşturulmuştur. Akışın türbülanslı olduğu kabul edilmiştir. Türbülans denklemlerinin çözümü için farklı türbülans modelleri denenmiş, yapılan ön analizler sonucunda kω-SST türbülans modelinin kullanımının daha uygun olduğuna karar verilerek yapılan tüm analizlerde kω-SST türbülans modeli kullanılmıştır. Yapılan akustik incelemeler için ise, Ffowcs-Williams ve Hawkins denklemleri (FW-H) kullanılmıştır. Zamana bağımlı denklemlerin sayısal olarak incelenmesi sırasında "second order impicit" yaklaşımı tercih edilmiş, diferansiyel denklemlerin ayrıklaştırma işlemi sırasında ise "second order upwind" yöntemi kullanılmıştır.

Bu çalışmada ele alınan susturucu modelinin sayısal olarak incelenmesine başlamadan önce, literatürde bulunan benzer geometriye sahip benzer çalışmalar belirlenmiştir. Bu çalışmaların geometri ve sınır şartları kullanılmış ve doğrulama analizleri yapılmıştır. Bu kapsamda literatürde bulunan iki farklı çalışma belirlenmiş, birisi aracılığı ile hesaplamalı akışkanlar dinamiği (HAD) yaklaşımının, diğeri ile ise hesaplamalı aeroakustik (HAA) yaklaşımının doğrulaması yapılmaya çalışılmıştır. Yapılan karşılaştırmalar sonucunda elde edilen sonuçların literatür ile uyumlu olduğu görülmüştür. Dolayısıyla bu çalışmada kullanılan sayısal yöntemlerin ve analizler sonucunda elde edilen sonuçların güvenilebilir seviyede olduğu düşünülmüştür. Ayrıca incelenen her geometri tipi için farklı eleman sayılarına sahip ağ yapıları oluşturularak deneme analizleri yapılmış ve her geometri için birer optimum ağ yapısı belirlenmiştir. Ek olarak farklı zaman adımları için deneme analizleri yapılarak, optimum ağ yapısı belirlenmiştir. Yapılan tüm sayısal analizlerde belirlenen optimum ağ yapıları ve optimum zaman adımı kullanılmıştır.

Bu çalışma kapsamında incelenen susturucunun perde tipi değiştirilerek farklı susturucu model geometrileri oluşturulmuştur. Bu kapsamda düz, konik, kavisli, L tipi ve Y tipi perde geometrileri belirlenerek beş farklı susturucu geometrisi belirlenmiştir. Bu modellerin perdesiz, tek perdeli, üç perdeli ve beş perdeli durumları için sayısal incelemeler yapılmıştır. Ayrıca kavisli perdeye sahip geometri için, susturucunun uzunluğu ve çapı değiştirilerek farklı susturucu boyutları için ek incelemeler yapılmıştır. Bu analizler sonucunda, incelenen modellerin akış, ısıl ve akustik karakteristikleri belirlenerek birbirleri ile karşılaştırılmıştır. Bu sayede basınç

düşümünün ve ses azalışının optimum gerçekleştiği, susturucu engel tipi ve susturucu boyutları belirlenmeye çalışılmıştır.

Çalışma sırasında ilk olarak, susturucu kullanılmamış bir silahın akış ve akustik analizi yapılarak, susturucusuz durum için basınç ve ses seviye değerleri belirlenmiştir. Belirlenen bu değerler, çalışma sırasında yapılan diğer analizler için bir referans noktası olarak kullanılmıştır.

Çalışmanın sonucunda düz, L tipi, konik ve kavisli beş adet perdeye sahip susturucu modellerinin susturucusuz duruma göre olan basınç düşüşleri sırasıyla %75,45, %79,75, %79,55 ve %81,3 olarak belirlenmiştir. Susturucu geometrisine 5 adet Y tipi perde sığdırılamaması nedeniyle, 5 adet Y tipi perdeye sahip susturucu için incelemeler yapılamamıştır. Bu nedenle 3 adet Y tipi perdeye sahip model geometrisi, susturucusuz durum ile karşılaştırılmış ve susturucusuz duruma göre %78,33 basınç düşüşünün gerçekleştiği tespit edilmiştir. Bu çalışmada ele alınan parametre aralığında, kavisli perdeye sahip susturucu kullanımının incelenen diğer perde tiplerine sahip susturuculardan daha iyi bir akustik performans gösterdiği tespit edilmiştir. Bu nedenle kavisli perdeye sahip susturucu için, susturucu çapı ve boyutları değiştirilerek ek incelemeler yapılmıştır.

Yapılan analizler sonucunda, beş adet kavisli perdeye sahip susturucu geometrisi için maksimum çıkış basıncı 3,748 MPa olarak elde edilmiştir. Beş adet kavisli perde sayısı sabit tutularak, susturucu çapı 1/6 oranında arttırıldığında maksimum çıkış basıncı 3,4961 MPa, susturucu uzunluğu 1/6 oranında arttırıldığında ise maksimum çıkış basıncı 3,3636 MPa olarak belirlenmiştir. Susturucunun hem çapı hem de uzunluğu 1/6 oranında artırıldığında ise maksimum çıkış basıncının değeri 3,177 MPa olarak elde edilmiştir. Dolayısıyla perde sayısı değişmeden, susturucunun boyutlarının artırılmasının basınç ve ses düşüşüne sebep olduğu gözlemlenmiştir.

Bu çalışmada incelenen parametreler aralığında, bir silahta susturucu hiç kullanılmadığı durumda 169,498 dB ses basınç seviyesi elde edilmiştir. Aynı silah ve şartlarda, silaha perdesiz bir susturucu takıldığında ise 162,134 dB ses basınç seviyesi belirlenmiştir. Susturucu içerisine bir adet, üç adet ve beş adet kavisli perde eklendiği durumlarda ise, ses basınç seviyesinin değeri sırasıyla 160,234 dB, 159,437 dB ve 158,117 dB olarak tespit edilmiştir. Beş kavisli bölmeye sahip bir susturucu

için, susturucu çapı 1/6 oranında artırıldığında ses basınç seviyesi susturucusuz duruma göre 16,515 dB azalarak 152,983 dB olarak belirlenmiştir. Susturucu uzunluğu 1/6 oranında artırıldığında ise 17,541 dB değerinde bir azalış gerçekleşmiş ve ses basınç seviye değeri 150,956 dB olarak elde edilmiştir.

Çalışılan parametre aralığında en çok ses azalmasının sağlandığı susturucu geometrisi, beş adet kavisli perdeye sahip ve susturucunun hem çapının hem de uzunluğunun 1/6 oranında arttırıldığı susturucu geometrisi olarak belirlenmiştir. Bu susturucu geometrisi için elde edilen değerler susturucunun hiç kullanılmadığı durum ile karşılaştırıldığında sıcaklık değerinde 484,86 K azalma ve ses basınç seviyesinde ise 20,835 dB değerinde bir azalma gözlemlenmiştir. Başka bir değişle bu susturucu geometrisi susturucusuz geometri ile kıyaslandığında sıcaklık değeri %32,32, ses basınç seviyesi değeri ise %12,29 azalış göstermiştir.

Sonuç olarak susturucu geometrisinin boyutlarının, kullanılan perde sayısının ve perde geometrisinin susturucu performansı üzerinde oldukça etkili olduğu gözlemlenmiştir. Susturcunun içinde yer alan perde sayısının ve susturucu boyutlarının artırılması ile susturucu çıkışında oluşan maksimum basıncın azaldığı, dolayısıyla oluşan ses seviyesinde de bir azalış gerçekleştiği gözlemlenmiştir.

Anahtar Kelimeler: Akış gürültüsü, kω-SST türbülans modeli, Akustik zayıflama, Aşırı basınç azaltma, susturucu, Ffowcs Williams-Hawkings akustik teorisi

ACKNOWLEDGEMENTS

I am deeply grateful to my supervisor Dr. Tolga DEMIRCAN for his assistance at every research stage and his insightful comments and suggestions.

Additionally, I would like to express gratitude to Dr. Hakan ARSLAN for his treasured support, which influenced my numerical methods. I also thank Mr. Elisha Apatewen AKANBONG, Mr. Bahadır GEMİCİOĞLU, and Kemo CAMARA for their continuous support. My appreciation also goes to my family and friends for their encouragement and support throughout my studies.

Lastly, I would like to thank the YTB for sponsoring my study and Prof. Dr. Yahya DOĞU, the Department Head of Mechanical Engineering at Kırıkkale University.

TABLE OF CONTENTS

LIST OF FIGURES

NOMENCLATURE

a_0	Speed of sound in the far-field (m/s)
Co	Sound velocity (m/s)
F1, F2	Production limiter
H(f)	Heaviside function
K	Turbulence kinetic energy (J/Kg)
N	Maximum number of iteration /time step
P	Pressure (Pa)
P_{ij}	Compressible fluid stress tensor (Pa)
P’	Fluid pressure in acoustic field (Pa)
R_L	Reynolds number
Sgs	Subgrid-scale model
t	Time (s)
T	Temperature (K)
T_{ij}	Lighthill viscus stress (Pa.s)
Ts	Time step size (ms)
U	Velocity (m/s)
Vt	Kinetic eddy viscosity (m^2/s)
Δ	Grid size (mm)
□(f)	Dirac delta function
μ	Eddy piscosity (Pa.s)
ρ	Density (Kg/m^3)

LIST OF ABBREVIATIONS

BOP	Blast overpressure
CAA	Compitational aeroacuestics
CFD	Computational fluid dynamics
Co. B	Conical baffle
CVB	Curved baffle
DNS	Direct numerical simulations
F-WH	Ffowcs-Williams and Hawkins equations
HVAC	Heating ventilation and airconditioning
LB	L-shape baffle
LES	Large eddy simulation
NS	Navies stokes equation
OSPL	Overall sound pressure level
PSD	Power spectral density
RANS	Reynolds-averaged Navier–stokes
SB	Stright baffle
SPL	Sound pressure level
URANS	Unsteady reynolds-averaged Navier stokes

1. INTRODUCTION

1.1. What is sound?

Waves are formed while energy travels through a medium like water or air. Waves are classified into longitudinal (pressure) and transversal waves. A sound wave is a longitudinal wave in which the disturbance travels in the same direction as the wave (The Science of Sound, nd). Sound is a change in pressure, density, and temperature propagating through a medium like air or water. The speed of sound depends mainly on the sound medium in which the waves propagate and environmental conditions. Temperature, pressure, and other external factors influence the interactions between sound waves and particles.

Gunshot noise is a combination of several acoustic waves generated by four main components: the muzzle wave of the gunpowder, the shock wave generated by the supersonic motion of the projectile, the air column ejected from the gun barrel in front of the projectile, and the acoustic wave caused by the collision of weapon parts during the firing process (Guo et al., 2013; Hristov et al., 2015; Selech et al., 2020). The noise generated by the muzzle wave of gunpowder can be reduced by attaching a suppressor to the weapon to allow the exhaust gases to expand before being released into the atmosphere. Attunating this noise by using a suppressor was the main focus of this study.

When a weapon is fired, a large amount of noise is produced, propagating as a blast or shock wave. The extent and intensity of the noise vary greatly depending on the size and type of the weapon. The strength of the blast wave increases when muzzle energy increases (Lo et al., 2011; Selech et al., 2020). The noise generated by a firearm has adverse effects on structures, human bodies, and the environment. Noise can cause hearing damage and other health effects (e.g., high blood pressure, nerve disorders, etc.), impair speech, disrupt sleep, and affect children's academic performance. Also, it alters wildlife behavior, reduces property values, and affects historical and archaeological sites through structural vibrations.

1.2. Background of a suppressor

Overpressure suppression devices for firearms have long been known and used since the 19th century. Hiram Percy Maxim, an American inventor, invented and sold the first commercially successful suppressor in 1902. On March 30, 1909, he got his intellectual property rights (Keith Hudson et al., 1996).

1.2.1. Why use a suppressor?

A suppressor can reduce the temperature and pressure of the gas at the barrel outlet by providing a large volume for gas expansion. The suppressor also allows the gas to be released slowly into the atmosphere: this slower, more controlled release at a lower pressure results in lower sound pressure. The only way to eliminate the noise is to reduce the gas pressure from the discharge pressure to atmospheric conditions, which is almost impossible to achieve.

Pulling the trigger of a weapon starts a series of events that results in the discharge of one or more bullets. The trigger releases a firing pin, which strikes a cartridge and usually contains a primer, powder, and shot. The primer fires up and burns the powder, causing the projectile to exit the cylinder. The ignition creates high temperatures and high pressure. The propellant gas that follows the shot as it leaves the barrel produces the muzzle blast. The pressure wave has a loud noise when it comes into contact with the external environment (Murphy et al., 2018). Suppressors are used to reducing the noise generated by the muzzle blast. For maximum efficiency, silencers must be specially designed to allow the weapon gases to expand in the chambers.

Four processes determine the effectiveness of a suppressor (Lo et al., 2011):

1. It should cool the muzzle gases to a temperature that quenches the burning gases and prevents re-ignition later.
2. It should gradually mix the muzzle gases with air to prevent the oxygen in the air from supporting combustion.
3. It should slow down the muzzle gases to prevent the formation of a shock front.
4. It should hold back the gases until they become cool by expansion to prevent a temperature rise at the shock front.

One of the four processes or a combination of them must be incorporated to have a good sound suppressor. Cooling occurs when the gas flow is controlled in a heat sink long enough to transfer heat by convection and conduction or by adiabatic expansion in a variable area flow channel. Gradual mixing can be achieved by progressive venting downstream. Slowing down and retention can be achieved by changing the cross-section of the directional flow passage. No specific procedures or data exist for designing a sound suppressor for a particular weapon.

Suppressors are used for different purposes in large and small caliber weapons. The primary goal of overpressure reduction for heavy guns is to decrease the impact of the massive explosion on structures and supporting vehicles. The primary purpose of suppressors for small-caliber firearms is to minimize the effect on hearing by reducing the magnitude of the blast (Keith Hudson et al., 1996; Rehman et al., 2011).

According to Maccarthy et al. (2011), using moderators has several advantages. Such as hearing loss and tinnitus prevention, increased accuracy (in many but not all cases), restricting the capacity of the barrel to blow on shooting and influencing gas release in the wake of a leaving projectile, and a decrease in perceived recoil (by up to 40%), and limited disturbance to livestock, particularly hunting animals. The disadvantages mentioned in this study are the possibility of falling on criminals, the additional cost and weight of the Silencer, shifting the center of gravity further away from the weapon user, and an undesirable moment of force.

Most sound suppressors use the same configuration introduced by Hiram Maxim in 1910. An expansion chamber is used first, then a series of baffles follows. The shockwave first travels through the expansion chamber, which traps most of the initial high-pressure gas in a fixed-volume space. Now moving more slowly, this gas continues to follow the projectile and fills the distance between the individual baffles. When the gases leave the moderator, they have slowed down and become trapped to such an extent that they no longer emit a loud sound (Maccarthy et al., 2011).

When a projectile accelerated by high-pressure and high-temperature gunpowder gas fires out, a muzzle blast wave of high-intensity sound pressure is generated. The level of impulsive noise increases as the weapon system's muzzle energy increases. The study of noise levels at different distances from the test site confirmed that impulsive

sounds could be heard from ten miles away (Guo et al., 2013). In contrast to other types of sounds, the noise produced by firearms has so many unique characteristics and properties like high energy, high amplitude, short duration, impulsivity (Huerta-Torres et al., 2021; Per Rasmussen et al., n.d.), long-range propagation, and high directivity (Rehman et al., 2011). These unique characteristics allow it to reach out to communities and surrounding neighborhoods easily. A muzzle blast wave is due to the gas pressure produced by the powder.

The positive impulse duration for large-caliber guns is a few milliseconds; The positive pulse duration for small-caliber gun systems could be less than 0.5 milliseconds (Foltz, 2019; Hristov et al., 2018; Huerta-Torres et al., 2021). In general, impulse noise from the small-caliber firearm is centralized in the 500-1000 Hz frequency range, whereas impulse noise from heavy guns is concentrated in the low-frequency range, mostly less than 200 Hz. Many studies on suppressor development have attempted to reduce the frequency of gunshot noise (Hristov et al., 2018; Lo et al., 2011).

Due to the association with the strong instability at the barrel exit, The muzzle flow field produced by a supersonic projectile is highly complex (Zhang et al., 2013). Just after the shot is fired, the gases emitted from the muzzle of a weapon are usually accompanied by an intense lightning flash known as a muzzle flash. As a result, the primary flash is nothing more than an extension of the barrel's hot, highly pressurized gas. The escaping gases expand adiabatically and cool due to the large ratio of muzzle gas pressure to atmospheric pressure, causing the luminosity to disappear and a dark zone to form. At this point, the gases are overexpanded and then decompressed by passing through a shock front. This recompression increases the temperature of the gas (Klingenberg & Mach, 1976).

Therefore, a suppressor is necessary to control the secondary combustion and the shock wave of the muzzle flow (Li & Zhang, 2021). After the bullet exits the gun, a high-pressure, high-temperature gunpowder gas is released into the surrounding air. This gas generates an unstable flow, resulting in various undesirable phenomena such as pressure, sound, blast, electromagnetic waves, muzzle, and smoke. Furthermore, the precursor flow field generated by expulsing a column of air from the barrel in front of

the projectile complicates the muzzle flow due to the precursor gas shock (le Roy, 2011).

Flow phenomena like compression waves, expansion waves, shear layers, shocks, and pressure waves complicate the fluid flows around the muzzle of a gun barrel (Hristov et al., 2015, 2018); as muzzle energy increases, impulse noise increases (Hristov et al., 2018).

Based on the attachment with the barrel suppressor can be classified into two. The most common one is the external or muzzle-mounted suppressor, which can be easily attached to and removed from the barrel using a thread or coupling device. The integral Silencer is an alternative silencer that is fitted around the barrel. In most cases, holes are drilled in the barrel to allow the gas to enter the silencer housing. The problem with integral suppressors is fouling the suppressor by unburnt propellant gas.

Many things affect the performance of the Silencer either positively or negatively.

1. Changing the position of the silencer ports in the barrel
2. Changing the silencer volume and
3. Changing the size of the openings in the barrel wall

1.2.2. The principles behind a suppressor

A suppressor is based on three principles that can be combined to create the most effective model for the situation (Aimée Lister, 2006).

1. Energy Absorption
2. Energy Dissipation
3. Energy Containment

1.2.2.1. Energy Absorption

Heat is transferred from the hot propellant gas to the cool metal of the Silencer and its contents by using energy-absorbing devices such as wire mesh. As with the design of the muffler, the wire mesh interrupts the gas column and serves as a heat sink to cool the hot gas. This heat transfer reduces the ability of the gas to do work by reducing

its energy, thus reducing noise emission. Maximizing surface area and using a heat sink helps to optimize heat transfer. The gas can escape from the barrel into the chamber, where the wire mesh absorbs it. As the temperature of the gas decreases, its pressure decreases, and so does the noise level.

1.2.2.2. Energy Dissipation

In dissipative devices, the gas does work to lower its total energy before it is released into the atmosphere. It can be done by viscous shear on the channel walls or by moving a device such as a rotor. This method has disadvantages, such as difficulties in design and manufacture and torque generation for the weapon.

1.2.2.3. Energy Containment

Containment devices consist of chambers in which the gas can expand. The gas expands, reducing the energy concentration and allowing the gas to escape at a lower pressure and velocity, thus reducing noise. Initially, silencer designs required many closely spaced baffles to achieve maximum performance. However, methods have changed, and today small silencers with wider spacing baffles are possible due to complex asymmetric designs.

Silencers are used extensively to reduce noise in various applications, including engine intake and exhaust systems, heating, ventilation, air conditioning (HVAC) systems, and compressors. Acoustic evaluation of silencer performance is therefore critical to their design, especially in the presence of flow.

1.3. Literature review

Keith Hudson et al. (1996) analyzed suppressors using the Navier-Stokes equation as the governing equation and a multispecies chemically reacting gas as a firing gas. Another research was also done by Rehman et al. (2011) with the same method and three straight baffles. Both cases observed a significant reduction in pressure and sound level.

The firing test and computational fluid dynamics (CFD) analysis were carried out by Lee et al. (2018) for a 40mm suppressor. The result agreed with the results of the shooting test. Zhao et al. (2019) also CFD and Computational Aeroacoustics (CAA) were used to calculate the muzzle flow field and jet noise for cases with and without silencers. Hristov et al. (2018) used the standard unsteady κ-ε turbulence model for overpressure reduction for the small caliber analysis, and a 74% reduction was achieved.

Arslan et al. (2020) theoretically and numerically, using the finite element method (FEM), and experimentally investigated the acoustic performance of a reactive multi-chamber muffler. According to this study's results, the baffles' geometry, the number of baffles, and the baffles' position influence the mufflers' performance.

The application of CFD to small caliber gun muzzles was investigated in the study of Cler et al. (2003) using a transient 2-D and mesh adoption to study the explosion. Because the main propellant flow of CFD results did not match, the study recommends using axisymmetric and 3-D grids when possible.

To assess the effect of the Silencer, Kang et al. (2008) examined the blast's pressure fluctuations in the flow field by the URANS equation, and a 42 dB attenuation of the sound pressure level was obtained.

Vehicle exhaust systems were studied by Tushar Chindha & Sanjay Bhaskar (2015) to reduce the noise generated by the combustion of fuel engines. The study also aimed to check whether the fluid flow causes the vibrations in the muffler or not. The study concluded that the vibrations are essentially due to the fluid flow.

The research was conducted by Aimée Lister (2006) to optimize the reactive Silencer. Several silencer configurations were introduced and studied. In this study, it was found that increasing the number of baffles and increasing the size of the holes in the barrel directly affected the effectiveness of a silencer.

Seçgin et al. (2021) study silencer's aiming to improve acoustic performance using extension tubes. The study optimizes the silencers' position, number, and extension geometry as design variables and the sound transmission loss as a response variable.

According to the study, increasing the baffling of a silencer and increasing the length of the extension tubes lowers the value of sound transmission loss.

1.4. Turbulence flow

Leonardo da Vinci carried out the first scientific study of turbulence (turbolenza) (lived 1452-1519). The Reynolds number of a flow determines whether it is laminar or turbulent. The Reynolds number equation can be written as follows (Uruba, 2019).

$$\mathrm{Re_L} = \frac{\rho . U . L}{\mu} \tag{1.1}$$

- The flow's length scale determines the Reynolds number.:

$$L = X, d, d_{hyd} \ldots \text{etc}$$

- The transition to turbulence is affected by the type of flow: around an obstruction: $\mathrm{Re_L} > 20{,}000$ and Internal flow: $\mathrm{Re_L} > 20{,}000$

Fluid compressibility is critical at high subsonic to supersonic/hypersonic speeds. When a compressible fluid is turbulent, thermodynamic fluid properties like density and specific entropy change, as do thermo-physical fluid properties like viscosity coefficient and specific heat (Zhipeng Lou, 2017). Experimental studies can provide valuable insights into the structure of turbulent flows but rely heavily on measurement techniques and are expensive. Therefore, numerical simulation and prediction of the structure and properties of turbulent flows are critical. Since turbulence is a random process, a perfect representation of turbulence effects is impossible in CFD simulations; instead, turbulence models are used. As there is no "one size fit" for all problems, selecting the most appropriate turbulence model for the simulation is necessary. The options for modeling turbulence from low to high accuracy are RANS (Reynolds-Averaged Navier Stokes), LES (Large-Eddy Simulation), and DNS (Direct Numerical Simulation). These three turbulence models are briefly described in the coming section.

Smith et al. (2017) compared LES to RANS-based CFD models for several combustion applications. The paper examines these two approaches' fundamentals, strengths, and limitations and recommends when each is most appropriate. An LES-based CFD tool simulates turbulent reaction chemistry combined with thermal

radiation transport in buoyancy-driven flames (i.e., gas flares) and the effect of large flames on surrounding objects (i.e., wind fence, process equipment, etc.). To summarize, RANS is mainly used to investigate internal combustion systems (i.e., process heaters) because the steady operation is more likely when the procedure operates in a controlled environment. On the other hand, LES has been demonstrated to be most applicable to external combustion systems (i.e., gas flares) because ambient conditions such as crosswinds can significantly influence the combustion process.

While LES is less expensive than DNS and performs well in flow separation regions, it is costly near the wall. RANS provides the most cost-effective method, with good predictive capabilities close to the wall and poor performance in flow separation regions. Combination RANS/LES simulation is an attractive alternative method for optimizing the advantages of RANS and LES models. A RANS modeling approach is utilized in the near-wall region, and an LES-based model is used in separated flow regions (Hanafi & Khlifi, 2016).

1.4.1. Reynolds-averaged Navier-stokes (RANS)

The Navier-Stokes equations are ensemble-averaged in the RANS modeling approach, all turbulent scales are modeled, and only the mean velocity is resolved (Alam, 2013). Since all turbulent scales are modeled, it is the most accessible approach and does not correctly account for all turbulent scales. It may require input from experimental data or additional calibration to be generally applicable.

The most commonly used RANS turbulence models are K-ε, K-ω, and Kω-SST. The difference between K-ε and K-ω is that K-ε calculates the flow in open space with high accuracy, while K-ω calculates the flow near the walls with high accuracy. The combination of these two models results in a new model known as Kω-SST (Hodor et al., 2017).

RANS simulations do not generate turbulent fluctuations but model turbulence effects. RANS models alone cannot predict noise, especially jet noise, because noise is fundamentally unstable and caused by turbulent fluctuations (Gong, 2012; Hudson et al., 2001). RANS turbulence models have an advantage in applications with high Reynolds number flows that exceed the current capabilities of LES and DNS LES and

DNS. Under these conditions, the wide range of spatial and temporal scales that constitute turbulent flow can be modeled in a steady-state simulation with RANS at a low computational cost (Blake, 2020).

1.4.2. Direct numerical simulation (DNS)

Direct numerical simulation solves the Navier-Stokes equations without turbulence modeling to obtain velocity fields in space and time. The DNS method provides accurate predictions by solving all turbulence spatial and spectral scales. DNS is the ultimate high-fidelity turbulence model, but calculating jet noise is expensive, even at low-to-moderate Reynolds numbers, due to the long simulation runtimes, large domains, and fine mesh requirements. DNS remains impractical for compressible and turbulent flows with high Reynolds numbers due to the wide range of temporal and spatial scales at these Reynolds numbers. As a result, DNS research has focused on lower Reynolds numbers (Alam, 2013; Araya, 2019; Blake, 2020; Gong, 2012; Yucetepe et al., 2015).

1.4.3. Large-eddy simulation (LES)

Large-eddy simulation (LES) is a mathematical model used in computational fluid dynamics for turbulence flow (Garnier et al., 2009). Joseph Smagorinsky first used this method in 1963 to simulate the flow of atmospheric air (James E. & Caskey, 1963). Deardorff extended in 1970 for general flow modeling (Deardorff 1970). Now a day, LES is used in a variety of engineering applications, like combustion (Pitsch et al., 2006), acoustics (Wagner et al., 2007), and boundary layer simulations of the atmosphere (Sullivan et al., 1994).

Large-eddy simulations solve a filtered version of the Navier-Stokes equations, accounting for unresolved turbulence through a subgrid-scale model. It is developed to improve RANS by capturing some of the flow scales. In LES, low-pass filtering (averaging the small length scale) is applied to the Navier-Stokes equations to remove the high-frequency wavenumber from the solution. Since the large scales of the flow (most responsible for momentum and energy transfer) are resolved, LES allows better accuracy than RANS. The small and computationally intensive scales, which play an essential role in dissipation, are modulated rather than resolved. Therefore, LES is

computationally cheaper than DNS and is suitable for simulating practical engineering problems (Blake, 2020).

Small scales are much more homogeneous and universal than large scales. And they are less affected by geometry and boundary conditions; they are much more likely to be universally modeled and require minimal adjustments when applied to various flow patterns than models for the RANS equations. Energy can be transferred instantaneously in both directions, from large eddies to small or small eddies to large eddies. The opposite way of transfer is referred to as "backscattering." Nevertheless, it is assumed that most energy is transmitted from large scales to subgrid scales, which relates to the classical theory of an energy cascade. According to this theory, the subgrid scales serve as an energy sink (Xu et al., 2003).

There are two types of LES filtering equations: implicit and explicit. Because the smallest scale (turbulent eddy size) dissipates in implicit filtering, the grid size becomes the low-pass filter. According to this implicit zonal description, the eddy viscosity near the wall region takes a value consistent with a RANS modeling approach, i.e., characteristic of Reynolds stress. In contrast, the eddy viscosity in separated flow regions takes on the value of an LES's subgrid stress (SGS) model (Alam, 2013; Sun & Domaradzki, 2018). Explicit filters reduce truncation errors by applying a pre-defined filter shape to the discretized Navier-Stokes equations. Explicit filters have a higher computational cost than implicit filters because they require finer resolution.

1.5. Computational aeroacoustics (CAA)

Computational Aeroacoustics (CAA) is the numerical simulation of noise generation and propagation problems. The two main simulation approaches are direct (simultaneous solution of fluid and acoustic fields simultaneously) and hybrid (acoustic waves are solved separately from the fluid flow). Within these two approaches, there are several methods, including acoustic analogies, semi-empirical methods, and computational fluid dynamics (CFD). Simulations based on CFD provide high fidelity, accuracy, and flexibility to predict both the flow field and the acoustic waves. It also allows in-depth analysis and the ability to directly investigate

the relationship between flow structures and acoustics in a way that experimental investigations can not (Blake et al., 2022).

Aeroacoustics deals with sound generated by aerodynamic forces or motions from the fluid flow. It is not by externally applied parties or movements like classical acoustics (Crighton, 1977). A CFD-CAA hybrid method was used by Zhao et al. (2019) (Zhao et al., 2019b) to calculate the muzzle flow field using large-eddy simulation (LES) and noise attenuation by Ffowcs Williams and Hawkings (FW-H). The Ffawcs Williams-Hawking method is limited as it does not consider reflection, deflection, or transmission. However, it provides upper and lower limits that can be used for engineering design (Hodor et al., 2017).

1.5.1. Transmission loss, insertion loss, and noise reduction

Noise reduction, transmission loss, and insertion loss are well-known techniques for evaluating sound attenuation performance. The difference in acoustic power before and after the Silencer is represented by noise reduction. Insertion loss compares the sound pressure level at a distance from the Silencer with and without the Silencer. Although relatively easy to measure, insertion loss and noise reduction are not necessarily suitable for evaluating sound attenuation performance because they are influenced by the impedances of the sound source and the radiation. Transmission loss is often used in assessing sound attenuators because it represents the acoustic performance of the Silencer alone based on the incident and transmitted waves (Kim, 2012).

1.6. Target

Suppressor designers are constantly trying to optimize the balance between size, weight, and noise reduction, using different methods. But most research in this area has focused on vibration analysis using the FEM method. Despite this, understanding why the overpressure created at the suppressor exists or how suppression methods work has not been adequately studied sufficiently by researchers.

Experiments do not show changes in the flow field caused by the muzzle brake, nor do they fully reproduce the evolution and propagation of the muzzle noise field. Advances at CFD make it possible to model the cavity environment and reveal details about the flow that is difficult to determine from experiments. However, compared to the researchers at FEM, little research has been done using CFD to study the gas flow inside the muffler. Most of these CFD-CAA studies focus on 2D and simple geometry with a limited number of baffles due to the computational power of transient simulation. But this work has investigated 3D suppressor geometries with different shapes and configurations of baffles.

Recent advances in computational power and CAA make numerical simulation methods more suitable for nozzle noise research. This computational simulation investigated how different geometries and operating parameters affect system performance optimization using hybrid CFD-CAA methods. The propellant flow in the near and far fields and the acoustics in the far field were analyzed using the hybrid CFD-CAA method.

2. MATERIALS AND METHODS

A suppressor is usually a hollow metal tube made of steel, aluminum, or titanium and contains expansion chambers (Silencer (Firearms) - Wikipedia, n.d.; White, 1998). However, this study did not consider the effects of material properties on the performance of the suppressor.

The suppressors were designed with two different lengths and diameters to see the effect of the volume of the suppressor. Also, five different baffle shapes were used to investigate the shape of baffles. Zero, one, three, and five baffles were utilized for each suppressor size to study the effects of the number of baffles. Eighteen geometries were analyzed, and an acoustic analysis was performed for some selected geometry with better overpressure reduction.

Kω-SST was first performed for the fluid flow analysis using commercial software fluent in obtaining instantaneous fluid data. The second step was acoustic analysis by Ffowcs-Williams and Hawking's equation (FW-H) method to construct the combustion noise source from the Kω-SST data.

Methos used for this study

1. The necessary information was collected by reviewing related works of literature. And the structural modes of the suppressors were designed by SOLIDWORK.
2. After drawing the geometry, fluid bodies for the proppant flow, suppressor flow, and far-field flow were introduced into the geometry in Ansys via Ansys Space Claim.
3. Mesh

- MultiZone mesh method mesh was used for the best accuracy.
- The advantages of hybrid meshing and local meshing were used.

4. A Kω-SST -based analysis of the specific gas flow was performed using Ansys.

The steps followed to perform the fluid analysis:

1. Transient pressure-based analyzes were chosen for this study.
2. The following command was used to activate the second-order unsteady solver.

/define models unsteady-2nd-order? Then yes

3. Then kω-SST was selected for the turbulent solver enable.
4. The ideal gas air was chosen as the material (in most previous studies, air with ideal gas properties was used as the propellant gas (Aimée Lister, 2006; Hristov et al., 2018; Özbektaş & Sungur, 2021; Rehman et al., 2011)).
5. Initial inlet and outlet boundary conditions were then introduced. Pressure and temperature of 20 MPa and 1500 K were used as inlet boundary conditions, while the far-field outlet boundary conditions were pressure and temperature of 1 atm and 300 K, respectively.
6. Choose second-order implicit formulation in the methods.

Save the selected hybrid initialization and computational activities in CDAT format for post-processing CFD

Set the appropriate time step size (1.5×10^{-6} seconds) and all required solution parameters.

7. Run Kω-SST until the flow becomes statistically stable.

Methods for acoustic analysis

The general procedure for performing an FW-H acoustic calculation in Ansys fluent was as follows:

1. Run the transient solution until the statistically stationary solution is achieved.
2. Activate the FW-H acoustic model and set the associated model parameters.

Setup → Models → Acoustics→ Edit...

3. Specify the source surface(s) and select the options for acquiring and storing the source data.
4. The receiver was specified at a distance of 30cm away from the outlet of the suppressor
5. The transient solution by the following command and continue the simulation for a sufficiently long time, then save the source data.

solution → run calculation

6. Calculate and save the acoustic signals.

solution → run calculation → acoustic signals...

7. Post-process the acoustic pressure signals.

results → plots → fft → edit...

3. GOVERNING EQUATIONS

3.1. Modeling turbulence

This chapter discusses the details of the Kω-SST -based non-dimensional compressible Navier-Stokes equations (NS) used in the study.

3.2. SST K-omega turbulence models.

The SST K-Omega turbulence model is a popular two-equation eddy viscosity model in aerodynamics. It combines the Wilcox k-omega and k-epsilon models. A blending function, F1, activates the Wilcox model near the wall and the k-epsilon model in free flow. This guarantees that the proper model is used throughout the flow field.

- The k-omega model is well suited for simulating the flow in the viscous sublayer.
- The k-epsilon model is excellent for predicting flow behavior away from the wall.

The Navier Stokes and continuity equations are (Jean DASSÉ, 2006):

Continuity equation

$$\frac{\partial \rho}{\partial t} + \frac{(\partial \rho U_j)}{\partial x_j} = 0 \tag{3.1}$$

Navier Stokes equation

$$\frac{(\partial \rho U_i)}{\partial t} + \frac{\partial}{\partial x_j}(\rho U_i U_j) = \frac{\partial}{\partial x_j}\sigma_{ij} + \rho g_i \tag{3.2}$$

Conservation of enthalpy

$$\frac{\partial}{\partial t}\rho h + \frac{\partial}{\partial x_j}(\rho U_j h) = -\frac{\partial}{\partial x_j} q_j + S \tag{3.3}$$

The variables are defined as follows:

- ρ is the density of the fluid considered
- U_j its speed in the direction j,
- $\sigma_{ij} = P\delta_{ij} - r_{ij}$ is the stress tensor,
- τ_{ij} Is the viscous stress tensor,
- P, the pressure,
- g_i is the acceleration of gravity,
- h the mass enthalpy of the medium,
- $q = \lambda \frac{\partial T}{\partial x_j}$ the conductive heat flow that follows Fourier's law,
- T is the temperature,
- λ thermal conductivity,
- S is the sum of the source terms by volume of energy due to radiative transfers, chemical reactions, and other additional energy inputs.

SST k-omega Governing Equation (Matyushenko & Garbaruk, 2016; Menter, 1994; Paeres et al., 2022; SST K-Omega Model -- CFD-Wiki, the Free CFD Reference, n.d.)

Kinematic Eddy Viscosity

$$m \times V_T = \frac{\alpha_1 k}{\max(\alpha_1 \omega, SF_2)} \tag{3.4}$$

$$v_t = \mu_t / \rho \tag{3.5}$$

Turbulence Kinetic Energy

$$\frac{\partial k}{\partial t} + U_j \frac{\partial k}{\partial x_j} = P_k - \beta^* k\omega + \frac{\partial}{\partial x_j}[(\nu + \sigma_k \nu_T)\frac{\partial k}{\partial x_j}] \tag{3.6}$$

Specific Dissipation Rate

$$\frac{\partial \omega}{\partial t} + U_j \frac{\partial \omega}{\partial x_j} = \alpha S^2 - \beta\omega^2 + \frac{\partial}{\partial x_j}[(\nu + \sigma_\omega \nu_T)\frac{\partial \omega}{\partial x_j}] + 2(1 - F_1)\sigma_{\omega 2}\frac{1}{\omega}\frac{\partial k}{\partial x_i}\frac{\partial \omega}{\partial x_i} \tag{3.7}$$

Closure Coefficients and Auxiliary Relations

F1 (Blending Function)

$$F_1 = \tanh\{\{\min[\max(\frac{\sqrt{k}}{\beta^* \omega y}, \frac{500\nu}{y^2\omega}), \frac{4\sigma_{\omega 2} k}{CDk\omega y^2}]\}^4\} \quad (3.8)$$

Note: F1 = 1 inside the boundary layer and 0 in the free stream.

$CDk\omega$

$$CDk\omega = \max(2\rho\omega^2 \frac{1}{\omega}\frac{\partial k}{\partial x_i}\frac{\partial \omega}{\partial x_i}, 10^{-10}) \quad (3.9)$$

F2 (second blending function)

$$F_2 = \tanh[[\max(\frac{\sqrt{k}}{\beta^* \omega y}, \frac{500\nu}{y^2\omega})]^2] \quad (3.10)$$

P_K (Production limiter)

$$P_k = \min(\tau_{ij}\frac{\partial U_i}{\partial x_j}, 10\beta^* k\omega) \quad (3.11)$$

$$\phi = \phi_1 F_1 + \phi_2(1 - F_1) \quad (3.12)$$

Where $\alpha_1 = \frac{5}{9}, \alpha_2 = 0.44, \beta_1 = \frac{3}{40}, \beta_2 = 0.0828, \beta^* = \frac{9}{100}$

$\alpha_{k1} = 0.85, \alpha_{k2} = 1, \alpha_{\omega 1} = 0.5, \alpha_{\omega 2} = 0.85$ (Matyushenko & Garbaruk, 2016)

3.3. FW-H acoustic analogy method

The main difficulty in numerically predicting sound waves is that sounds have much less energy than fluid flows. The Kω-SST turbulence model was used in this simulation to capture this flow field. The Ffowcs-Williams and Hawkings analogy was used to calculate sound propagation.

The Ffowcs-Williams and Hawkings equation (FW-H) is essentially an inhomogeneous wave equation that can be obtained by combining the continuity and Navier-Stokes equations (Ffowcs Williams & Hawkings, 1969).

The FW -H equation can be written as(ANSYS, 2022; Zhao et al., 2019).

$$\frac{1}{C_o^2}\frac{\partial^2 P'}{\partial t^2} - \nabla^2 P' = \frac{\partial^2}{\partial x_i\,\partial x_j}[T_{ij}H(f)] - \frac{\partial}{\partial x_i}\{[P_{ij}n_{ij} + \rho U_i(U_n - V_n)]\delta(f)\} + \frac{\partial}{\partial t}\{[\{[\rho_o V_n + \rho(U_n - V_n)]\delta(f)\} \quad (3.13)$$

$$H(f) = \begin{cases} 0, & f = 0 \\ 1, & \text{elsewhwre,} \end{cases}$$

$$\delta(f) = \frac{d}{df}[H(f)] \quad (3.14)$$

The variables are defined as follows:

- P' denotes the acoustic field fluid pressure,
- C_0 is the sound velocity,
- T_{ij} is the Lighthill stress tensor,
- P_{ij} is the compressible fluid stress tensor,
- U_n is the fluid velocity component normal to the surface f0,
- V_n is the surface velocity component normal to the surface,
- H(f) is the Heaviside function, and δ(f) is the Dirac delta function.

p' is far-field sound pressure ($p' = p - p_0$). $f = 0$ is a mathematical surface introduced to "embed" the external flow problem ($f > 0$) in an unconstrained space, which facilitates the use of generalized function theory and the free space green function to determine the solution. The surface ($f = 0$) corresponds to the surface of the source and can coincide with a body surface (impermeable) or a permeable surface of the body surface. n_i is the normal unit vector pointing in the direction of the outer region ($f = 0$), a_0 is the far-field speed of sound, defined as (Alkan & Atayılmaz, 2018)

$$T_{ij} = \rho U_i U_j + P_{ij} - a_0^2(\rho - \rho_0)\delta_{ij} \quad (3.15)$$

- P_{ij} is the compressive stress tensor. For a Stokesian fluid, this is given by

$$P_{ij} = P\delta_{ij} - \mu\left[\frac{\partial U_i}{\partial X_j} + \frac{\partial U_j}{\partial X_i} - \frac{2}{3}\frac{\partial U_k}{\partial X_k}\delta_{ij}\right] \quad (3.16)$$

3.4. Evaluation parameters of noise

The critical measurement for the pressure fluctuations of a sound wave as it propagates through the air is the sound pressure level (SPL) (Alkan & Atayılmaz, 2018; Zhao et al., 2019).

$$SPL = 20\lg\frac{P'}{P_{ref}} \quad (3.17)$$

Where p′ is the perturbation($P' = P_{mean} - P_{ref}$) and P_{ref}= is the reference sound pressure, which is usually equal to the minimum human auditory threshold, $P_{ref} = 2 \times 10^{-5}$ Pa.

The peak sound pressure level SPL peak is used to calculate SPL for weapon muzzle noise. As well as the overall sound pressure level (OASPL) [4]. SPL peak = is the SPL corresponding to the pressure-time curve's peak value, whereas OASPL is the sum of all frequencies (Zhao et al., 2019):

$$SPL_{peak} = 20\lg\frac{P_{peak}}{P_{ref}}, \quad \text{and} \quad OASPL = 10\log\left(\sum_i 10^{SPL_i/10}\right) \quad (3.18)$$

Where SPL_i is the sound wave pressure level from the i^{th} harmonic wave.

4. VALIDATION, GEOMETRY, MESHING, AND TIME STEP SIZE

4.1. Validation one

Hudson et al. (2001) investigated a suppressor with one straight baffle using experimental and computational fluid dynamics methods to attenuate the sound from the firearm. The study measured the pressure at six different locations with six pressure gauges. A validation analysis was carried out to confirm this method's usefulness. The results of the numerical method were compared with the experimental results of Hudson et al. (2001).

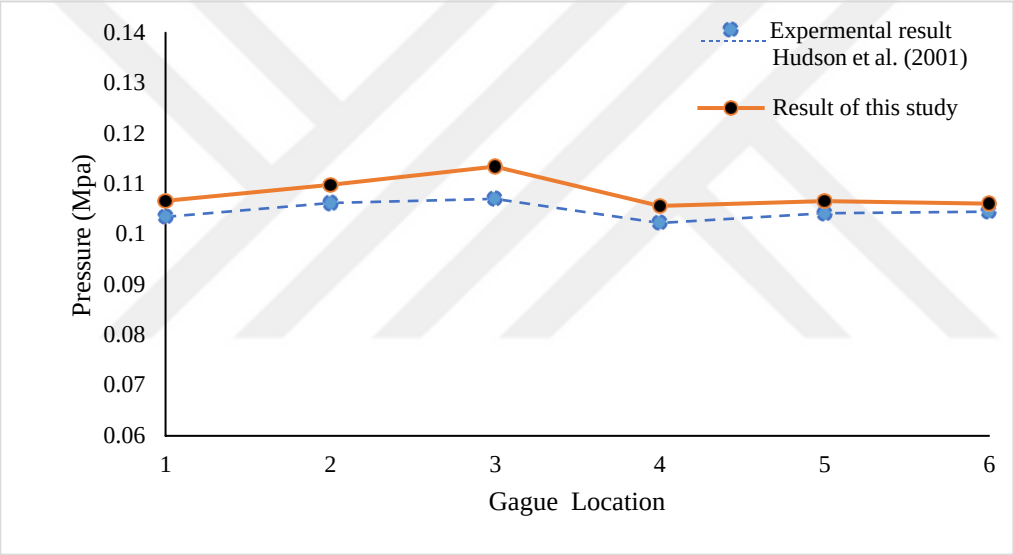

Figure 1. Peak pressure at the different locations

The maximum variation occurred at gauge location three, and the result of variation is presented in percentage as follows.

$$\text{Variation} = \frac{\text{Experimental Value - Numerical value}}{\text{Experimental value}} \times 100\%$$

$$= 5.6\%$$

The pick pressure at gauge three was compared with the numerical simulation results at the exact location. A vibration of 5.6% was recorded between experimental and numerical results. And the method was accepted as feasible for this case.

4.2. Validation two

The second validation analysis was done for the acoustic analysis by comparing the numerical result of the experimental development results made by Bozdemir et al. (2019). The acoustic validation analysis was done for both unsuppressed and suppressed conditions with 72×20 suppressors.

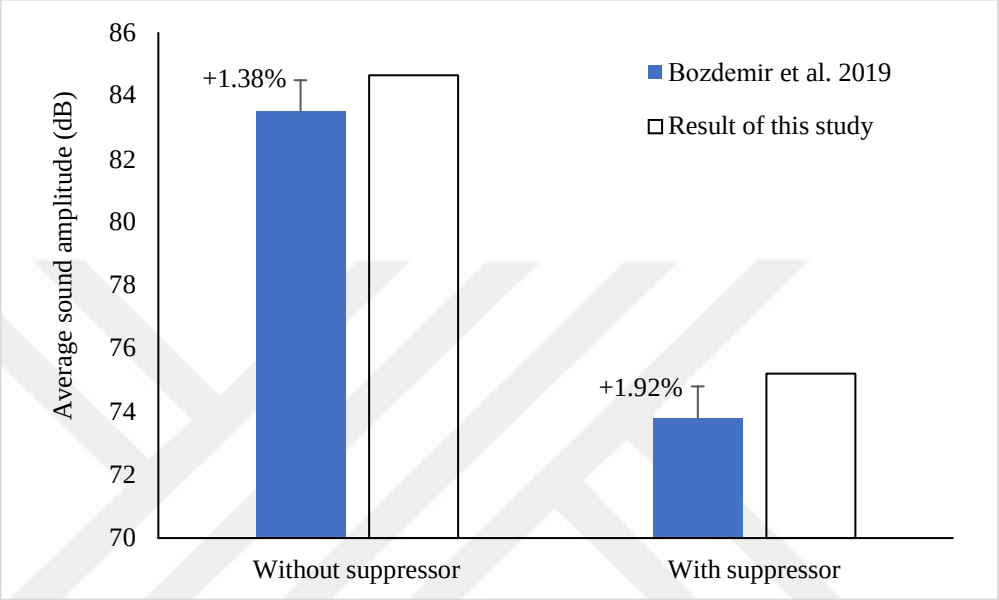

Figure 2. Average sound amplitude with and without the suppressor

In both suppressed and unsuppressed cases, the error of numerical analysis result compared to Bozdemir et al. 2019 was +1.38% and1.92%, respectively. This result shows that the numerical method is valid for such problems.

4.3. Geometry

This study compares Acoustic, overpressure, and temperature reduction analyses of suppressors. Suppressors with five different geometric deflector designs (straight, L-shaped, conical, Y-shaped, and curved) and zero, one, three, and five baffle configurations were studied. The outside suppressor size specified was 72×20, and the 3D model of the suppressor was done using SolidWorks. As the selected geometries are suitable for symmetry boundary conditions, half of the geometry was used in the study to reduce the computational cost. For the suppressor that shows the best performance, further analysis was done first by increasing the diameter by 1/6 to

analyze the effect of the increase in volume when the diameter increases. The second analysis was done by increasing the length by 1/6, keeping the other parameters constant, and the last by increasing the diameter and length by 1/6, keeping both the initial inlet and outlet boundary conditions constant.

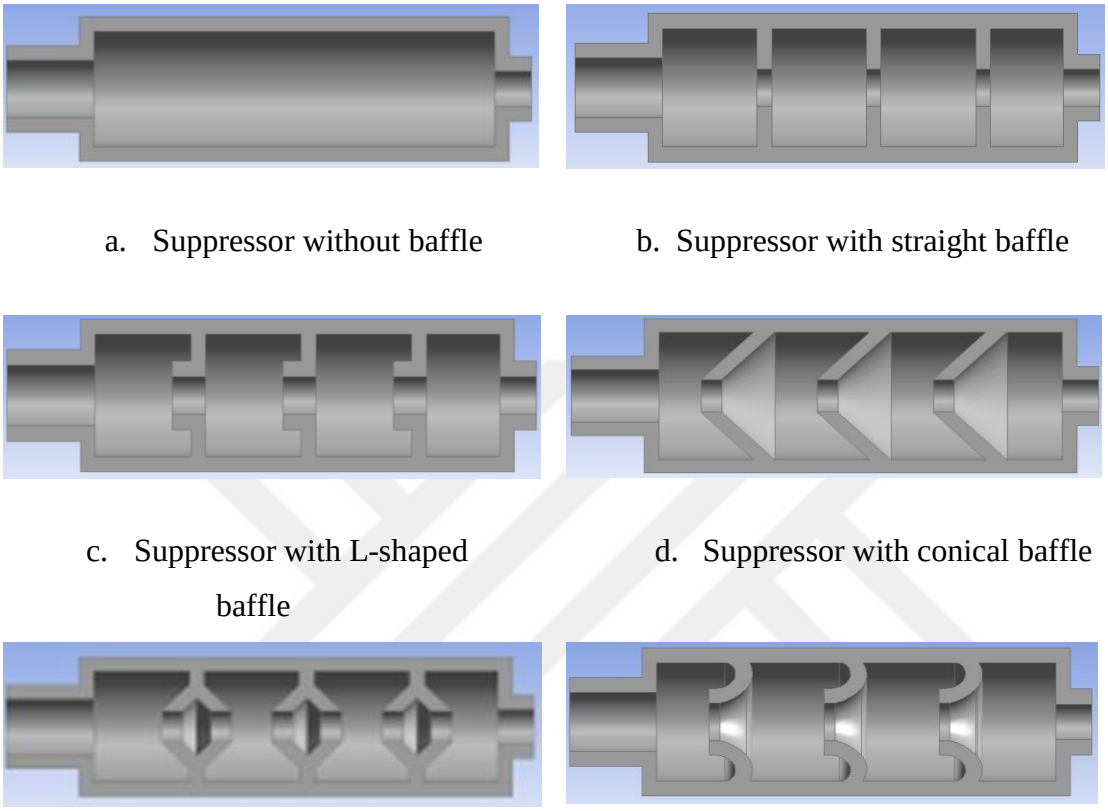

a. Suppressor without baffle

b. Suppressor with straight baffle

c. Suppressor with L-shaped baffle

d. Suppressor with conical baffle

e. Suppressor with Y-shaped baffle

f. Suppressor with curved baffle

Figure 3. CAD geometries of different suppressors

The outside dimension of the suppressor was taken from Bozdemir et al. 2019 (Bozdemir et al., 2019). The detailed dimension and the location of suppressors are presented in figure 4. When the number of baffles changes, the first expansion chamber keeps constant, and the last one (10mm) space is also constant

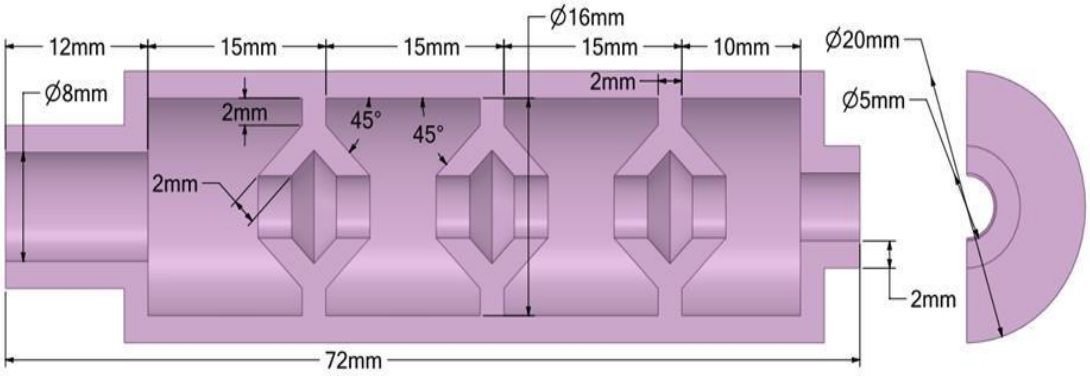

Figure 4. Suppressor detail dimension

For all geometries, a fluid body was introduced for both suppressor flow and far-field flow to analyze the blast wave outside the suppressor.

a. Without suppressor

b. Suppressor with straight

c. Suppressor with L-shaped Baffle

d. Suppressor with conical baffle

e. Suppressor with Y-shaped baffle

f. Suppressor with curved baffle

Figure 5. Suppressor and far-field fluids CAD representation

The analysis was made by keeping the far-field control volume constant and changing the types and dimensions of suppressor flow for the same initial inlet boundary condition. The control volume in the far-field should be large enough to give enough space for the gas to expand. Considering the room for gas expansion and computational cost, the dimensions chosen for the far-field control volume were 425mm by 90mm in length and diameter, respectively. From the total length, 25mm was for backflow. Since the jet flow is very directional, the far-field portion in front of the muzzle tip was separated from the rest to use local mesh sizing in this region. The size of this was equal to the diameter of the suppressor.

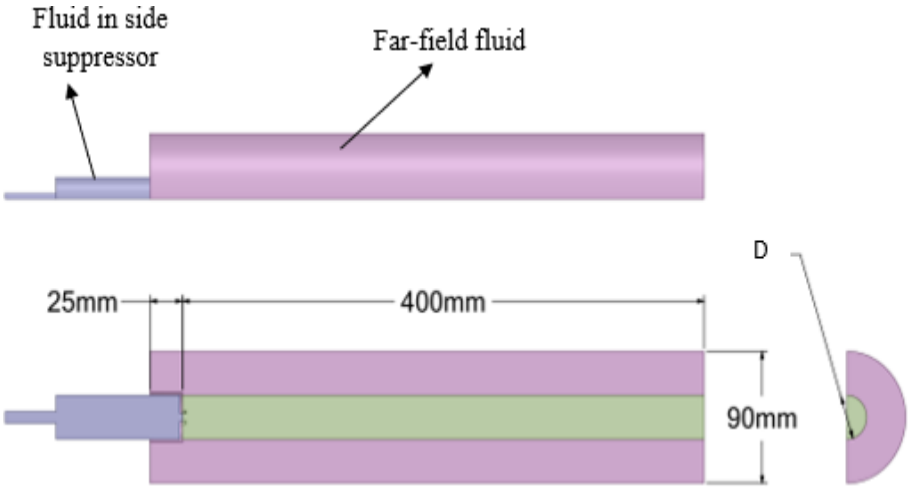

Figure 6. Dimension of the far-field control volume

Where D is the diameter of the suppressor

4.4. Grid size and time step

Assigning a suitable grid cell size and computational time step (ΔT) is very important to obtain accurate results from the simulation. The first step is to create a computational mesh with appropriate cell sizes for modeling. After generating a good computational mesh, the user must select a reasonable computational time step that works well with the mesh and the event being modeled. The appropriate time step is determined by the cell size and the flow velocity passing through those cells.

4.4.1. Sensitivity of the meshes

A trial-and-error mechanism was performed using several meshes and simulations until mesh independence was achieved. Body size, inflation, mesh refinement, MultiZone mesh method, and mesh adoption were applied to obtain a good quality mesh. The average orthogonal quality of the mesh was more than 0.92 for all geometries.

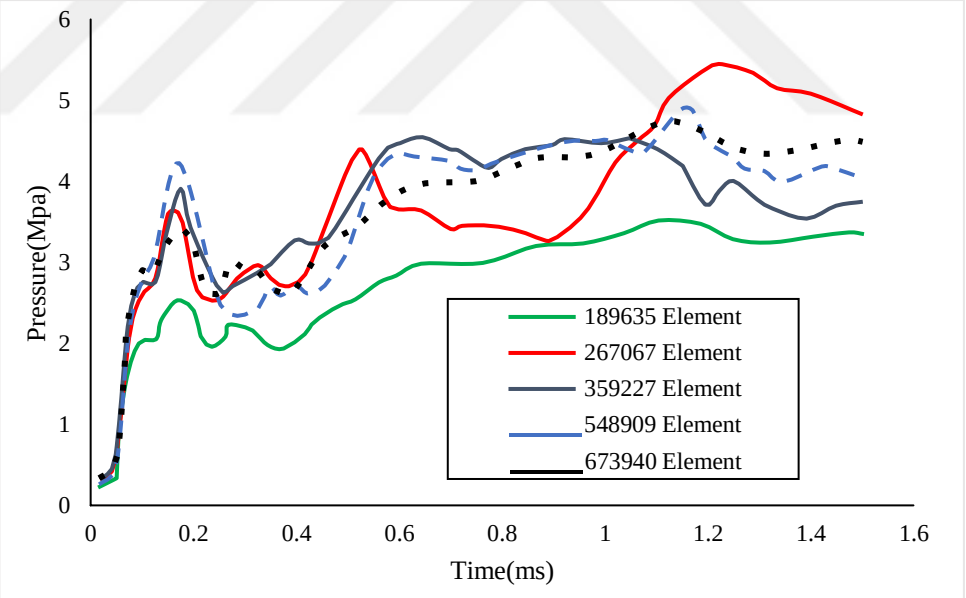

Figure 7. Pressure Vs. Time chart for different meshes

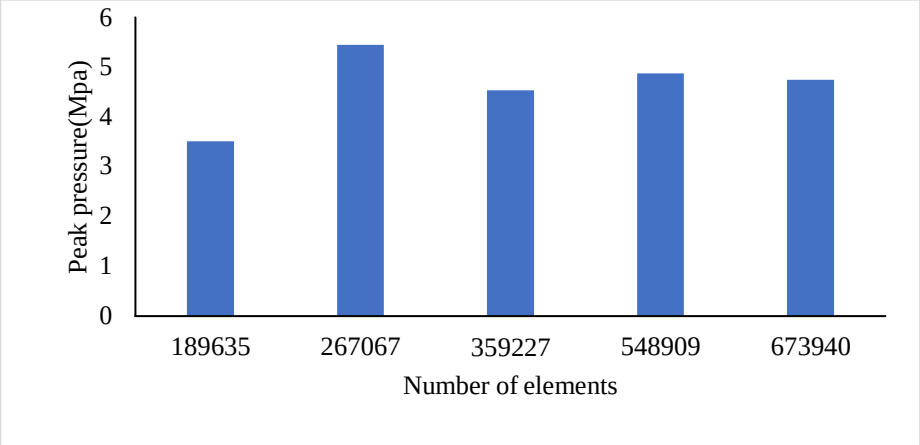

Figure 8. Pressure Vs. Number of element

The MultiZone mesh method decomposes the geometry automatically into mapped (structured/sweepable) regions and free (unstructured) regions. It generates a pure hexahedral mesh where possible. It then fills in the most difficult-to-capture areas with an unstructured multiZone mesh method, and the Sweep meshes method functions similarly. MultiZone, on the other hand, has capabilities that make it more appropriate for a class of problems where the sweep method would not work without extensive geometry decomposition.

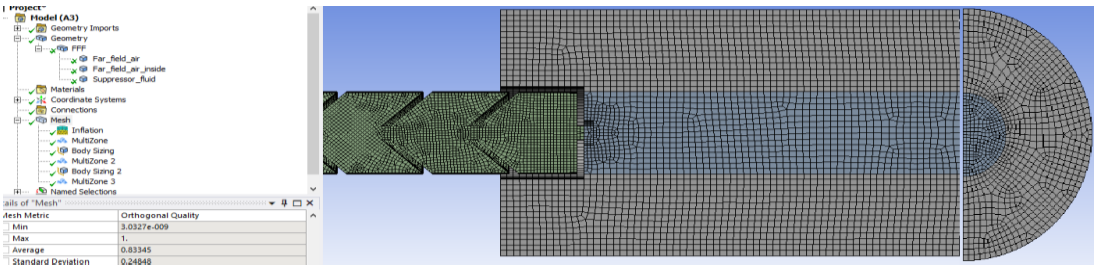

a. Front and side view of mashes

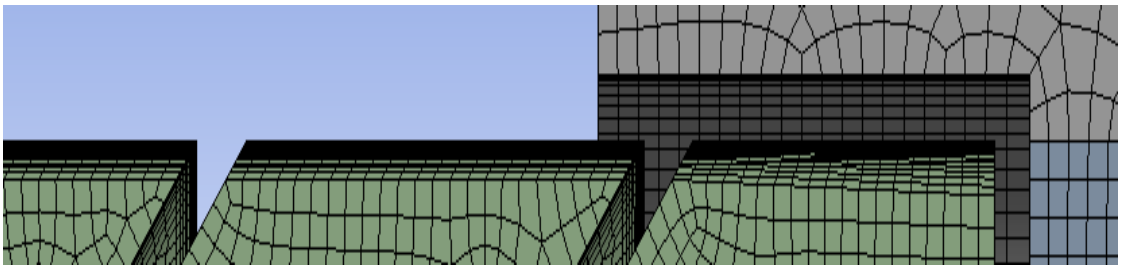

b. Mesh inflation

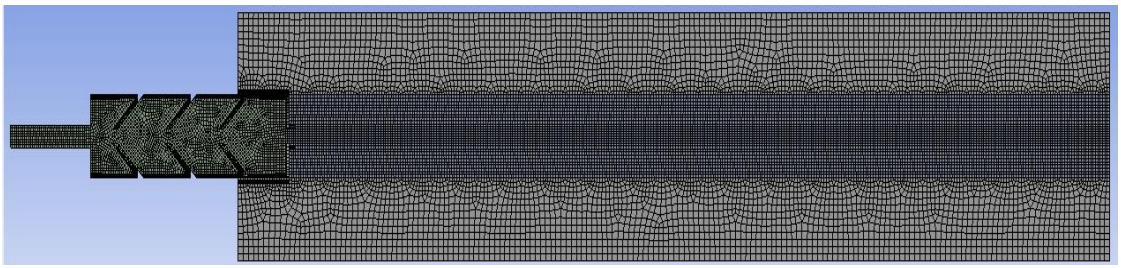

c. Suppress and far-field mesh

Figure 9. The meshing of suppressor fluid

Mesh structures starting from faces were created with 20 inflation meshes and an initial layer thickness of 0.00011448mm, which was determined with the y+ calculator to achieve y+=1.

Two different local scalings were used to consider the essential parts separately. Those are fluid inside the suppressor with a grid size of 0.7 mm. And for the fluid in the middle of the far-field control volume with a grid size of 0.9 mm. Global meshing was done with a maximum element size of 1.5mm and adaptive sizing.

4.4.2. Time step size and number of iterations

The size of the time step depends on the problem. It should be small enough to resolve the transient features correctly. The step size and the number of iterations specified for the solver affect the speed and accuracy of the simulation. If the step size is decreased or the number of iterations increases, the result becomes more accurate, but the simulation runs slower. If the step size increases or the number of iterations decreases, the simulation runs faster, but the result becomes less accurate.

To optimize your model for simulation on a real-time target computer, specify a combination of step size (Ts) and maximum iterations per time step (N) that provides acceptable accuracy and speed to avoid overrunning. The choice of ΔX and ΔT balances achieving good numerical accuracy and minimizing calculation time. Maximum iterations are the maximum number of iterations the solver will perform for each time step.

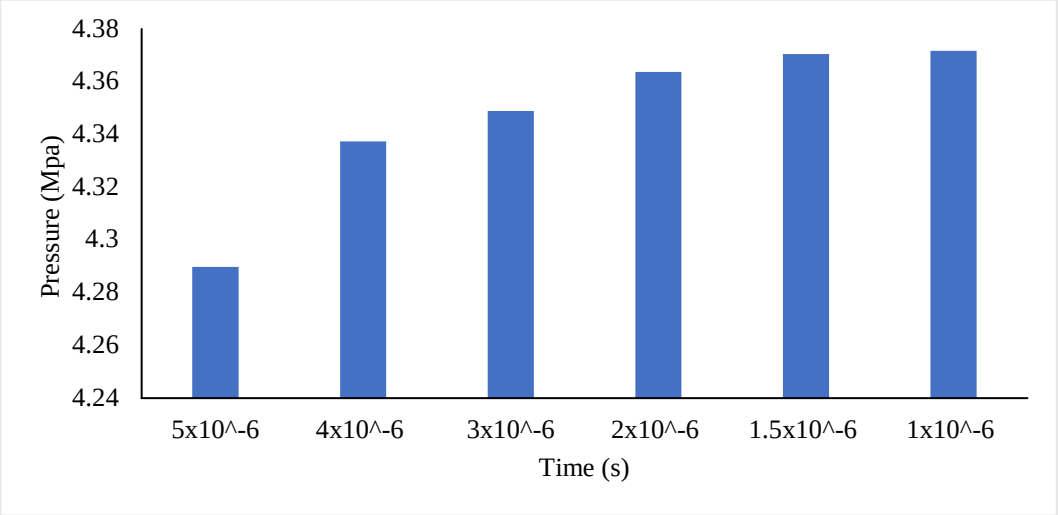

Figure 10. Pressure vs. time graph of time for time-independent analysis

After several trials, an optimum time step size of $\Delta T=1.5\times10^{-6}$second was selected for this study. As seen in Figure 10, after 1.5×10^{-6}second, the maximum pressure at the exit of the suppressor becomes constant.

Generally, in this section, the geometries were modeled by SOLIDWORKS. Then the validation of both turbulence and acoustics models was studied. In addition, the mesh and time-independent analyses were done by deciding the validity of the methods to increase the accuracy and precision of the results. After this, the turbulence flow and the acoustic analysis were done and presented in the coming section using the above methods for the modeled geometries.

5. RESULTS AND DISCUSSION

5.1. Modeling of the gas flow

The flow field in a suppressor was analyzed in terms of velocity, pressure, temperature, density distribution, and flow system. The compression of the overpressure drop with different methods and the characteristics of these methods are discussed. Several models were designed and simulated to determine which factor influences the attenuation of the sound during firing.

The following chart shows the Mach number of various suppressors with a single baffle. The Mach number varies from 1.56 in curved to 1.68 in L-shaped baffles. If the Mach number is higher than one, it is a supersonic flow. Supersonic flows are often characterized by shock waves that cause the flow characteristics and streamlines to change discontinuously, in contrast to the smooth continuous variation in subsonic flows.

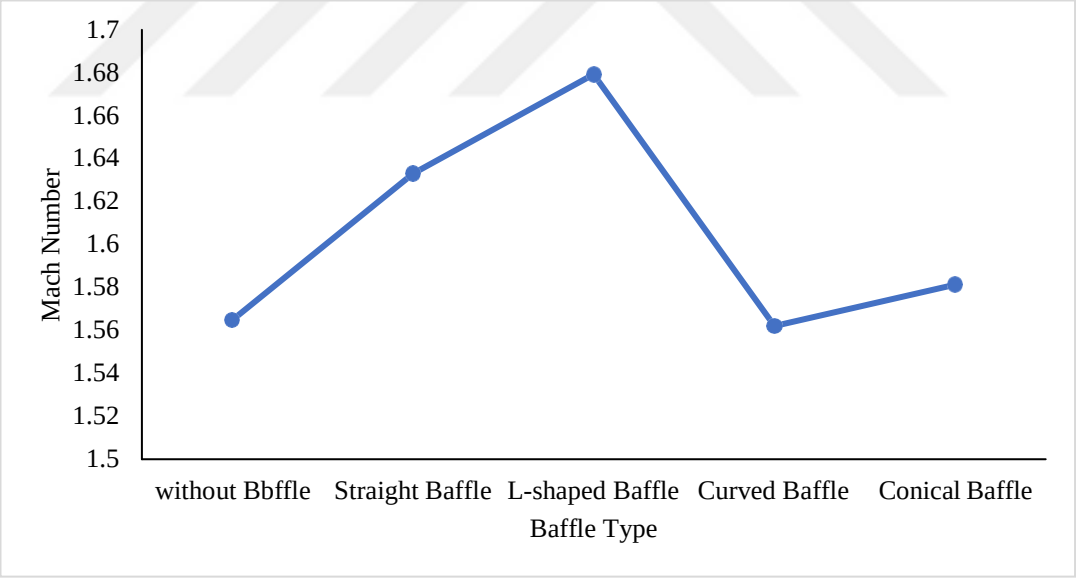

Figure 11. Mach number of different suppressors with one baffle

As shown in Figure 12, the baffle design creates a sequence of blast waves emitted from the suppressor during firing. From these flow characters, it can be seen that the blast wave is very directional. Due to this, the maximum pressure occurs in the axis of the suppressor.

Streamline graphs of different suppressors with one baffle and at a constant time are presented in this section. Also, to see how it changes with time, the study was done by keeping variables other than the time constant.

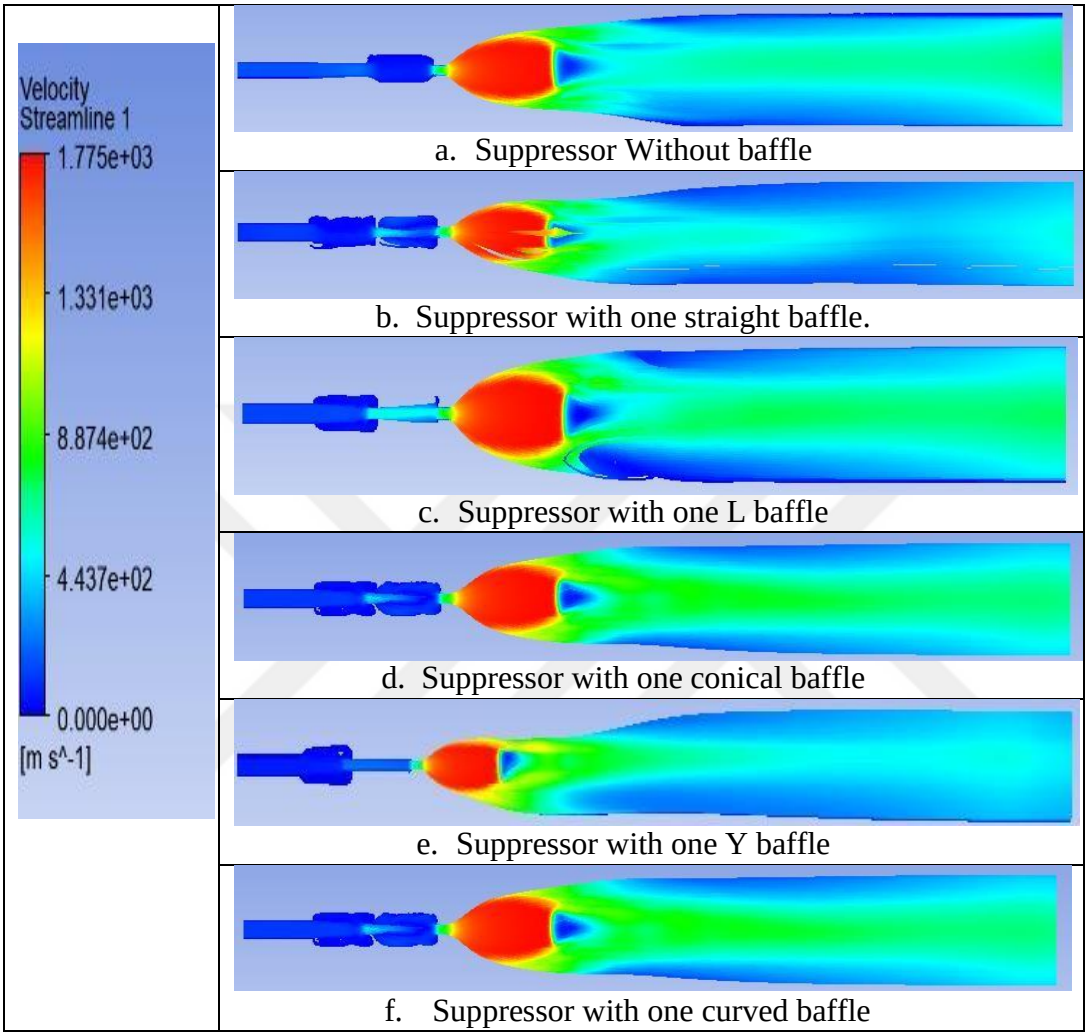

a. Suppressor Without baffle

b. Suppressor with one straight baffle.

c. Suppressor with one L baffle

d. Suppressor with one conical baffle

e. Suppressor with one Y baffle

f. Suppressor with one curved baffle

Figure 12. Bast wave streamlines of different baffles at 1.2 ms

From blast wave streamline of figure 12 was taken at a constant time of 1.2ms for all types of suppressors. This Figure shows that the baffle's shape considerably affects the waves created after the gun is fired and the amount of overpressure reduction.

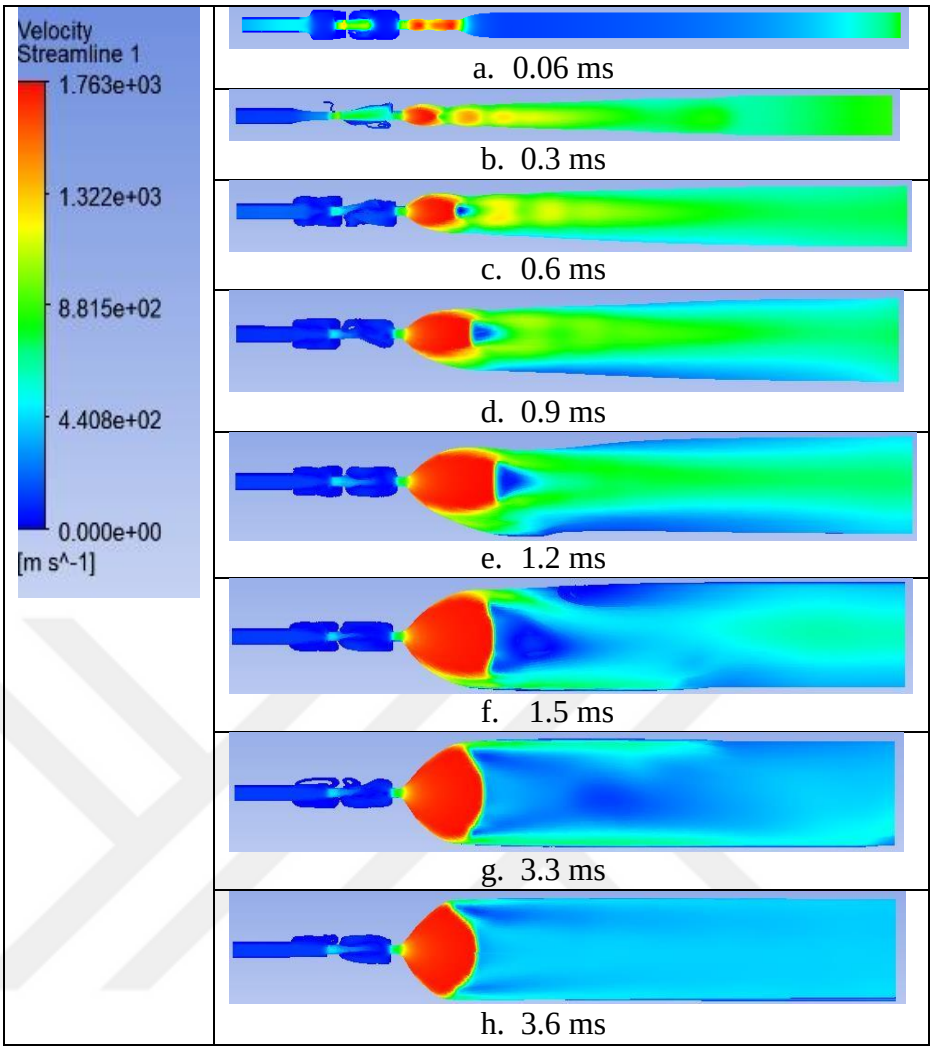

Figure 13. Transient changes in blast wave streamlines

In Figure 13, the blast wave was taken from the suppressor with one curved baffle. An oblique shock wave is inclined with respect to the incident upstream flow direction, as opposed to a normal shock wave. When a supersonic flow encounters a corner, the flow effectively turns in on itself and compresses.

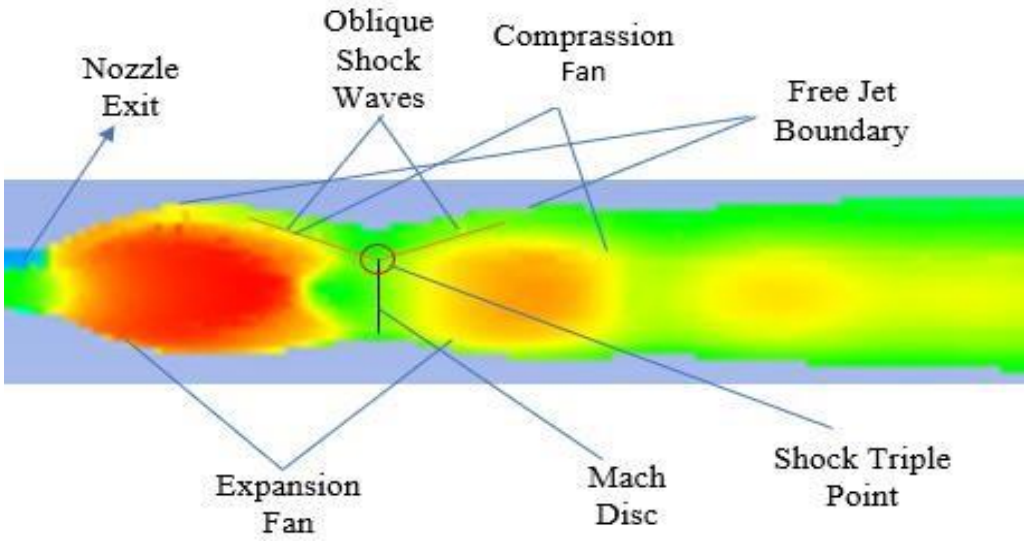

Figure 14. Shock wave structure in the near-field

Figure 14 was from a suppressor with a curved baffle at 0.3ms. The Figure shows that the exhaust gases do not all remain perfectly separated in the exhaust plume. When the flow exits from the suppressor, the outer edges of the blast wave start to mix with the surrounding air due to turbulence. When the exhaust gases are rich in fuel, the extra oxygen in the air reacts with the exhaust gases, resulting in more combustion. This picture shows the waves created at the exit of the suppressor during firing.

5.2. Analysis of suppressor with one baffle

The following section shows a detailed analysis of fluid properties such as pressure, temperature, density, and velocity. All these parameters were measured at the outlet of each suppressor.

5.2.1. Pressure analysis

Pressure reduction is crucial in aeroacoustics studies to attenuate the noise created by turbulent fluid flow. The section presents the overpressure reduction with the length of the suppressor for one baffled suppressor.

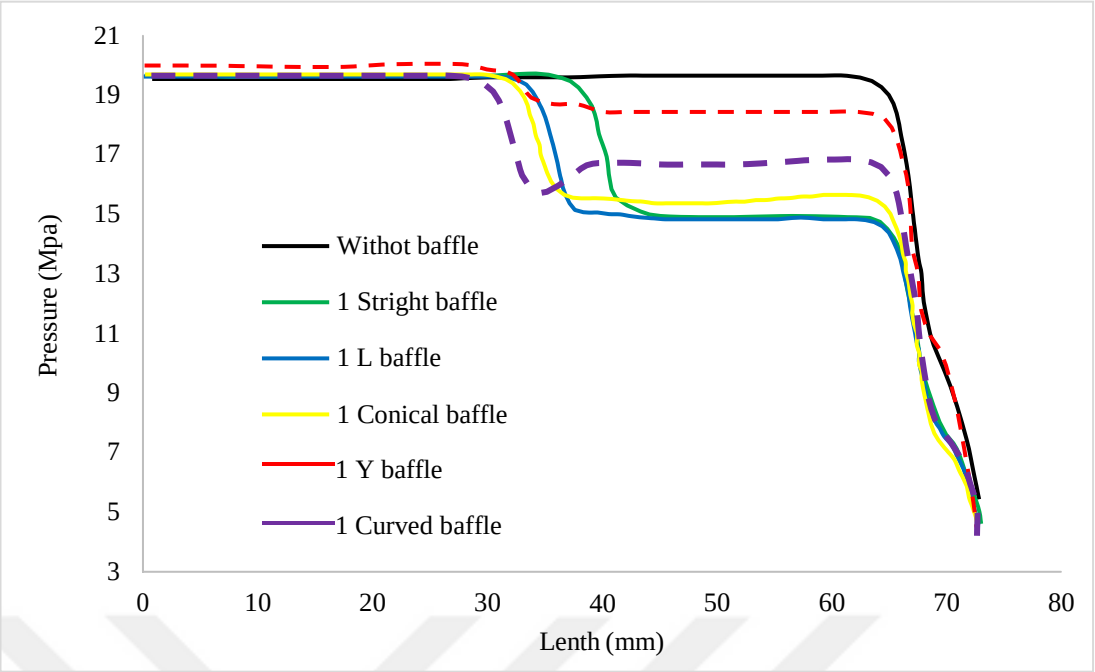

Figure 15. Pressure vs. length of suppressor with one baffle

Figure 15 shows the effect of baffles on the suppressors. From this graph, it can be concluded that using deflectors inside the suppressor increases the performance of the suppressor by reducing the overpressure. And Figure 15 also shows the suppressor's effectiveness when baffle type varies. Further analysis of the effect of increasing baffles on pressure reduction and other fluid properties is presented in the coming sections.

5.2.2. Acoustic analysis

5.2.2.1. Sound pressure level (SPL)

The pressure measured within the wave in contrast to the surrounding air pressure is known as sound pressure. Loud noises generate sound waves with high sound pressures, whereas quiet sounds generate acoustic signals having low sound pressures.

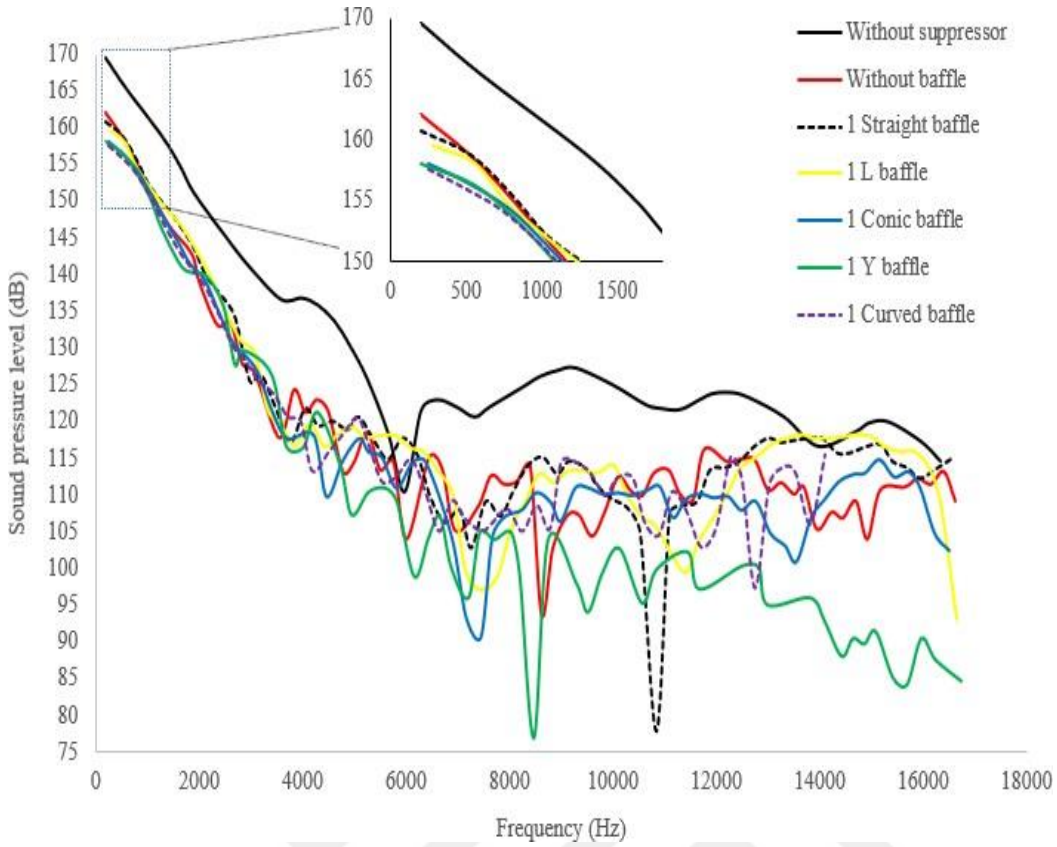

Figure 16. Sound pressure level vs. frequency for one baffled suppressor

Figure 16 shows the SPL of different suppressors with one baffle. The effectiveness also varies with the baffle type; complex geometries perform better, as seen in the Y, conical, and curved baffled suppressors. In unsuppressed conditions, the sound pressure level is around 170dB. Using suppressors with one baffle reduces the SPL value falls under 160dB. This reduction of SPL reduces the loudness of the explosion. As the loudness of the explosion decreases, the adverse effects of the noise also reduce.

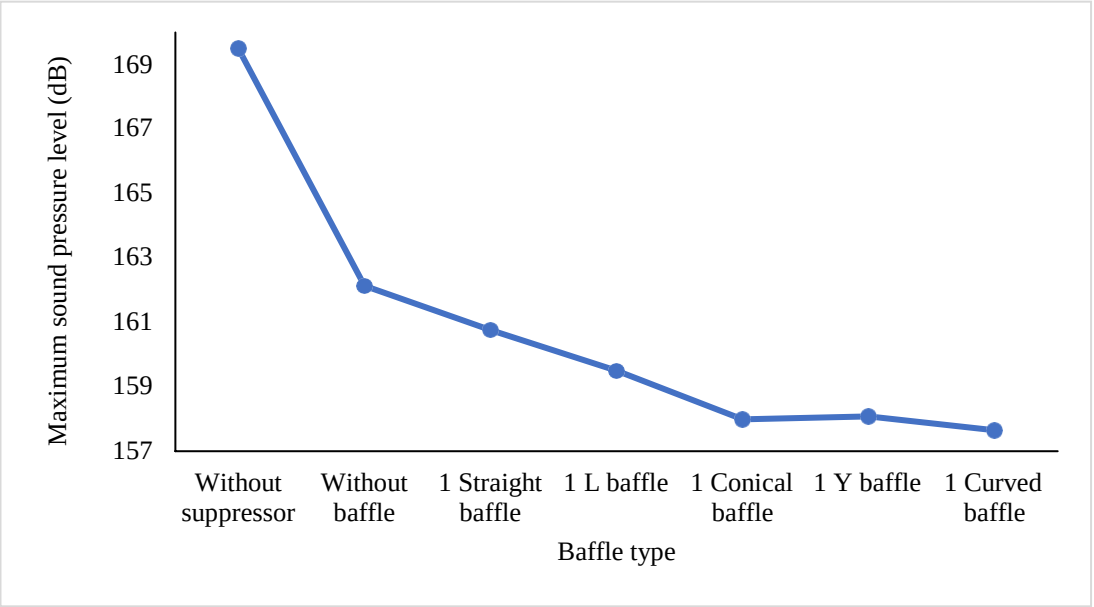

Figure 17. Maximum sound pressure level (SPL) vs. suppressor type

The maximum sound pressure level was the peak value for each suppressor, taken from the transient SPL chart. As seen in Figure 17 above, the maximum SPL decreases when using a suppressor and further decreases when the baffle is introduced inside the suppressor. The extent of reduction varies from baffle type to baffle type; according to this graph, curved baffle shows better attenuation.

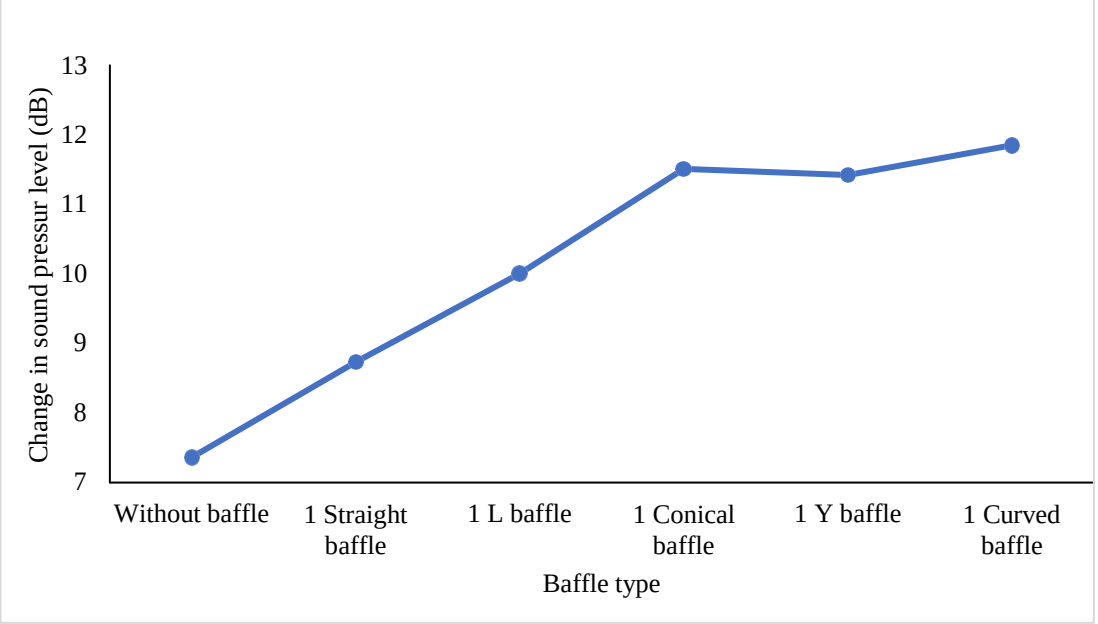

Figure 18. Change in sound pressure level (SPL) vs. suppressor with different baffle type

The change in sound pressure level is the difference between the maximum sound pressure level in unsuppressed conditions and suppressed conditions with different suppressors. As seen in Figure 18, the maximum change in SPL has occurred in the suppressor with the curved baffle.

5.2.2.2. Sound amplitude

The sound amplitude of an acoustic source is the measurement of the wave's height. The amplitude of a sound wave is described as its loudness or the amount of maximum displacement of the medium's vibrating particles from their mean location when the sound is created. The sound amplitude vs. frequency graph shows the maximum displacement of a sound wave's particles with respect to the number of vibrations made by a sound wave per second.

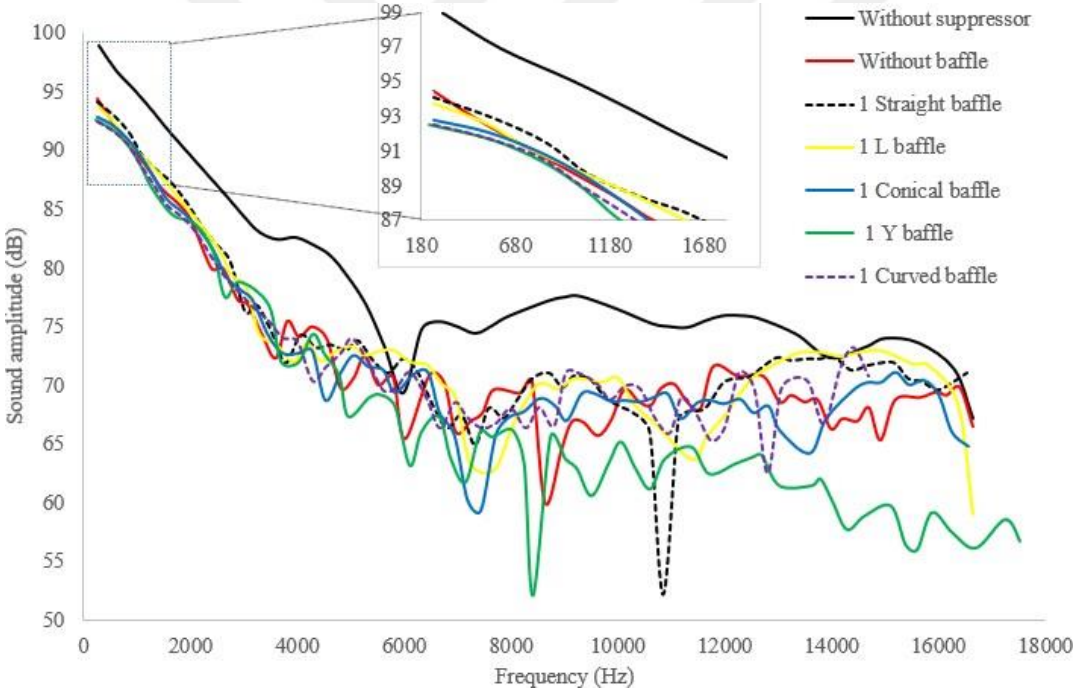

Figure 19. Sound amplitude vs. frequency

Figure 19 shows the sound amplitude of different suppressors with one suppressor. Suppressors having better overpressure reduction also have lower sound amplitude. When there is no suppressor, the sound amplitude reaches up to 99dB; higher amplitude results in louder noise. This graph shows that the sound amplitude decreases

using suppressors with and without baffles. However, using the baffle inside the suppressor further reduces this sound amplitude and improves attenuation.

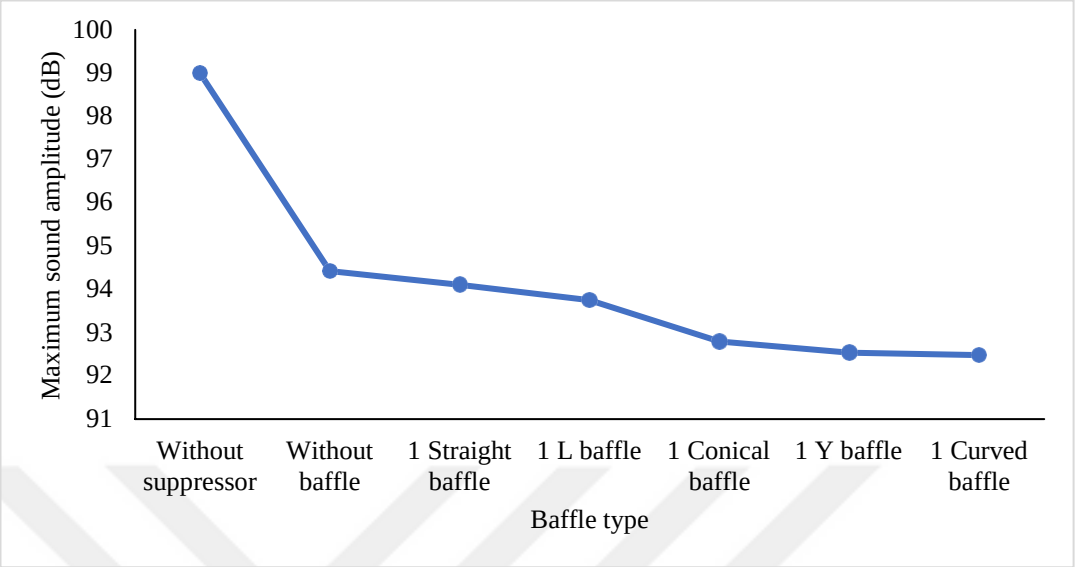

Figure 20. Maximum sound amplitude vs. suppressor type

The sound amplitude is transient and varies with time. The maximum sound amplitude is significant in designing a suppressor. The maximum sound amplitude of different firearm suppressors without a suppressor, suppressors without a baffle, and suppressors with varying shapes of the baffle are presented in Figure 20.

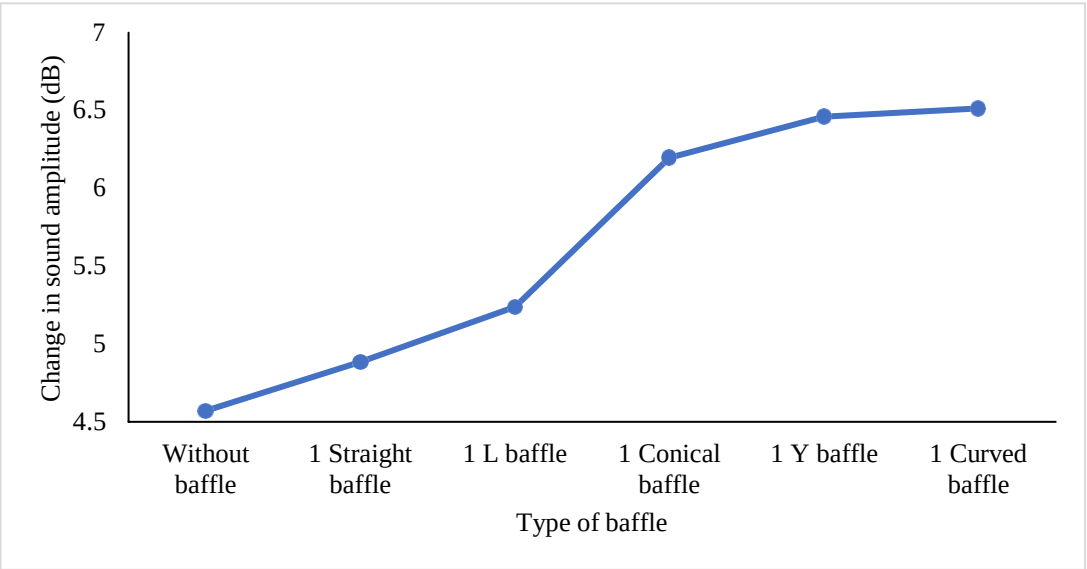

Figure 21. Change in sound amplitude vs. baffle type

Chang in sound amplitude is the difference between the maximum sound amplitude in the unsuppressed (without suppressor) condition and the maximum sound amplitude in suppressed (with suppressor) condition. Studying this change in sound amplitude helps to know the maximum attenuation of the sound compressor in contrast to unsuppressed conditions. As shown in Figure 21, the change in sound amplitude varies for different suppressors.

5.2.2.3. Power spectral density (PSD)

The power spectral density (PSD) is a visual representation of the distribution of signal frequency components. The power levels of the frequency components present in each are specified by power spectral density. Using the PSD profile, it is simple to identify the frequency components with relatively lower power levels in the given frequency range of interest(Dempster, 2001; Miller & Childers, 2004).

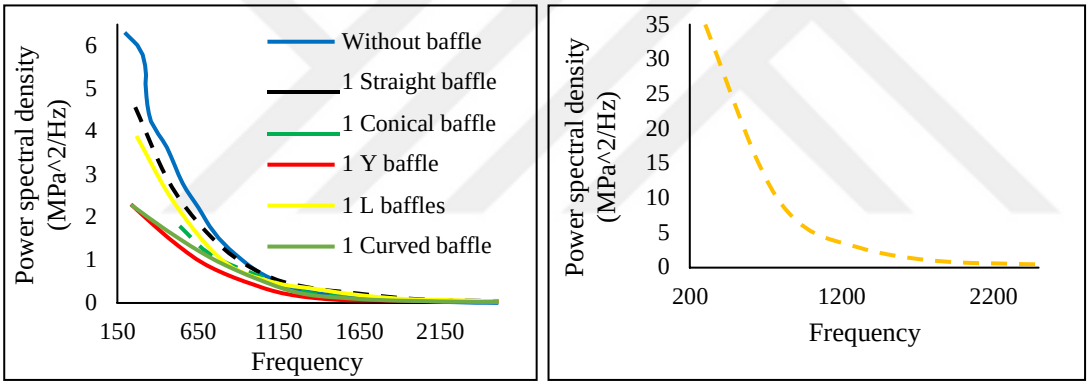

a. PSD with suppressor b. PSD without suppressor

Figure 22. Power spectral density (PSD)

Further studying PSD is essential in addition to SPL and sound amplitude because lowering PSD lowers the energy of the sound waves; this can be achieved by using suppression with complex shapes, as shown in figure 22.

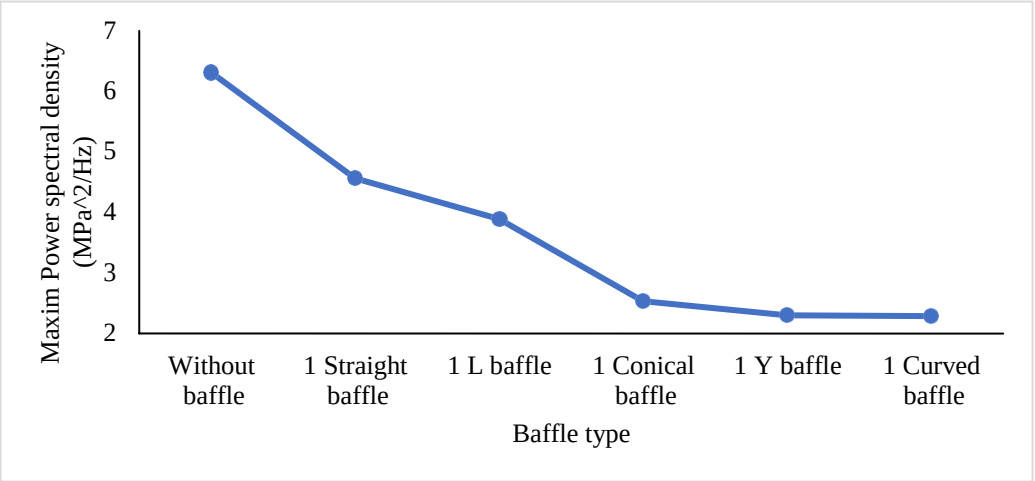

Figure 23. Maximum power spectral density for suppressors with different baffle types

Each frequency's power level decreases when the maximum power spectral density decreases, resulting in sound amplitude reduction. As seen in Figure 23, the power spectral density decreases when using a suppressor. It is also seen that using a baffle inside the suppressor reduces the power spectral density.

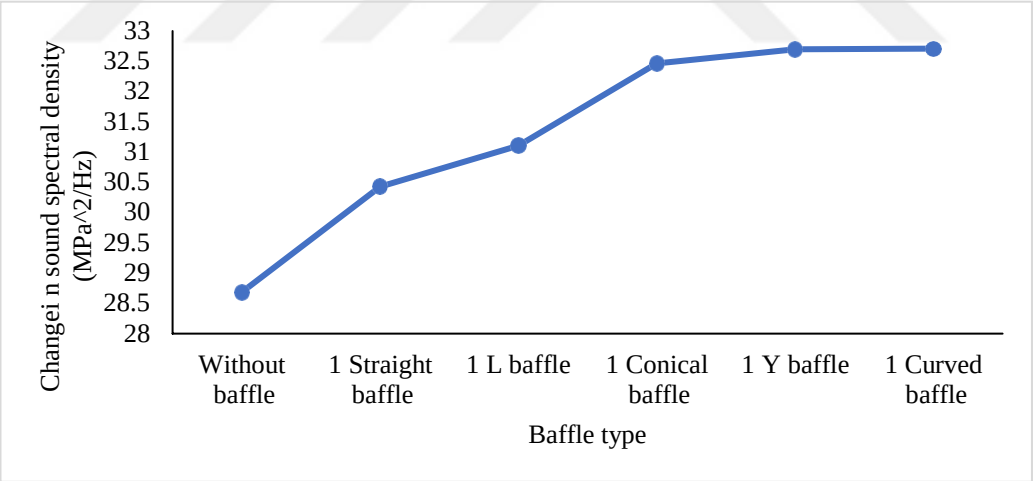

Figure 24. Change in power spectral density for suppressors with different baffle types

Change in power spectral density is the difference between maximum power spectral density in unsuppressed conditions and maximum spectral density in suppressed conditions. Like other parameters, change in power spectral density also varies when different baffles are used, as shown in Figure 24

5.3. Suppressor with different baffle shapes and baffle number

5.3.1. Pressure

Overpressure (also called blast overpressure) creates a shock wave greater than normal air pressure. A sonic boom or an explosion can produce a shock wave. Blast overpressure (BOP), also known as high energy impulsive noise, is a dangerous byproduct of explosives and weapon fire. BOP shock waves alone harm the hollow organ systems, most notably the auditory, respiratory, and gastrointestinal systems. (Elsayed & Gorbunov, 2007). This section discusses overpressure results regarding transient overpressure reduction, maximum, and change in overpressure reduction. The study was carried out by varying the number and shape of baffles.

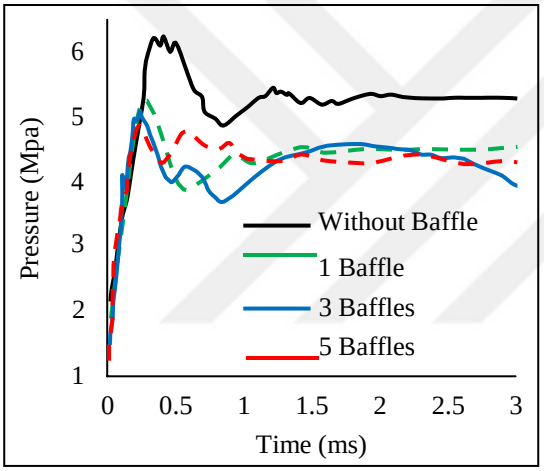

a. Straight baffle

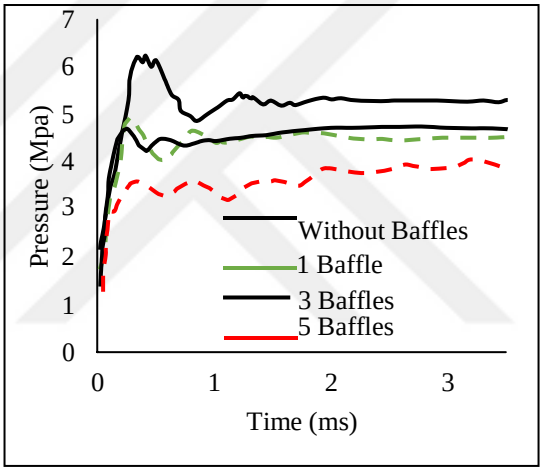

b. L-shaped baffle

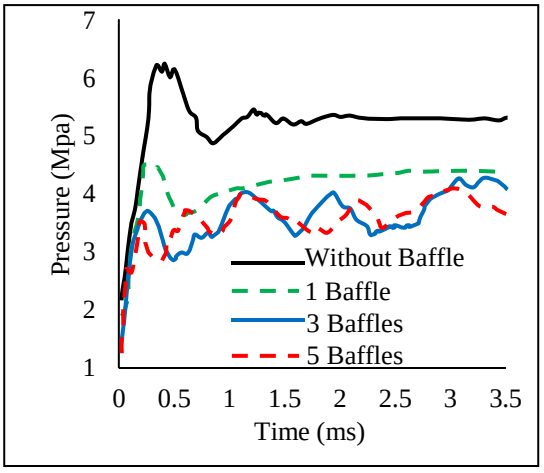

c. Conical baffle

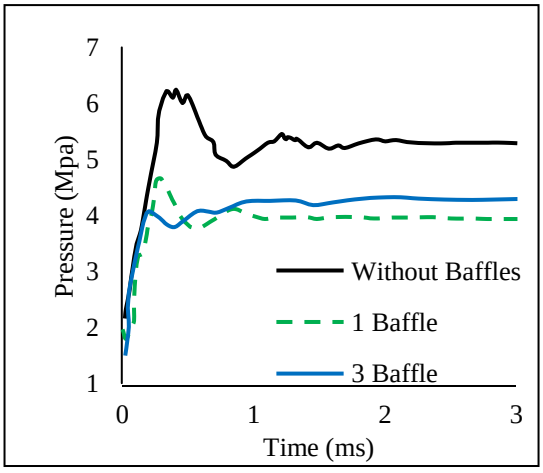

d. Y-shaped baffle

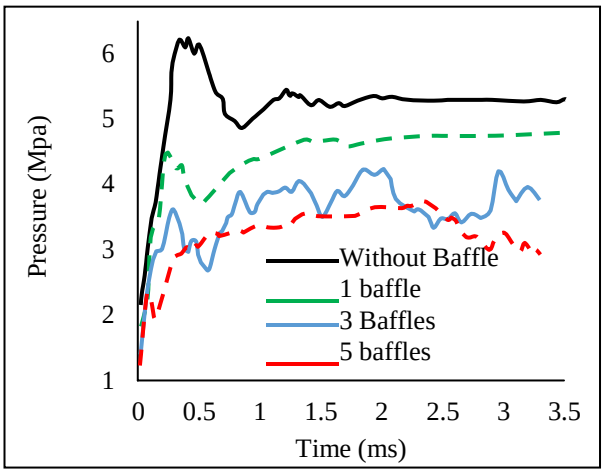

e. Curved baffle

Figure 25. Pressure vs. time graph of suppressors with different baffle

In both straight and L-shaped baffle suppressors, the overpressure reduction increased when the number of baffles was increased. The maximum pressure reduction straight and L-shaped baffle suppressors were 15.09Mpa (75.45%) and 15.95Mpa (79.75%), respectively, and it occurred when the suppressor was with five baffles.

The overpressure reduction of suppressors with five conical baffles was 15.91Mpa (79.55%) and for suppressors with three Y-shaped baffles was 15.676Mpa (78.33%). Because the size of the suppressor was insufficient, the analysis was not done for a suppressor with five Y-shaped baffles.

In a 20×72 suppressor with a curved baffle, the overpressure drop increased as the number of baffles increased. The percentage drop in overpressure for the suppressor with one, three, and five curved baffles were 76.01%, 78.79%, and 81.3%, respectively, compared to the initial value. This shows, like other suppressors, that the overpressure was reduced according to the size and number of baffles. The curved suppressor performed better than the other silencers examined in this study.

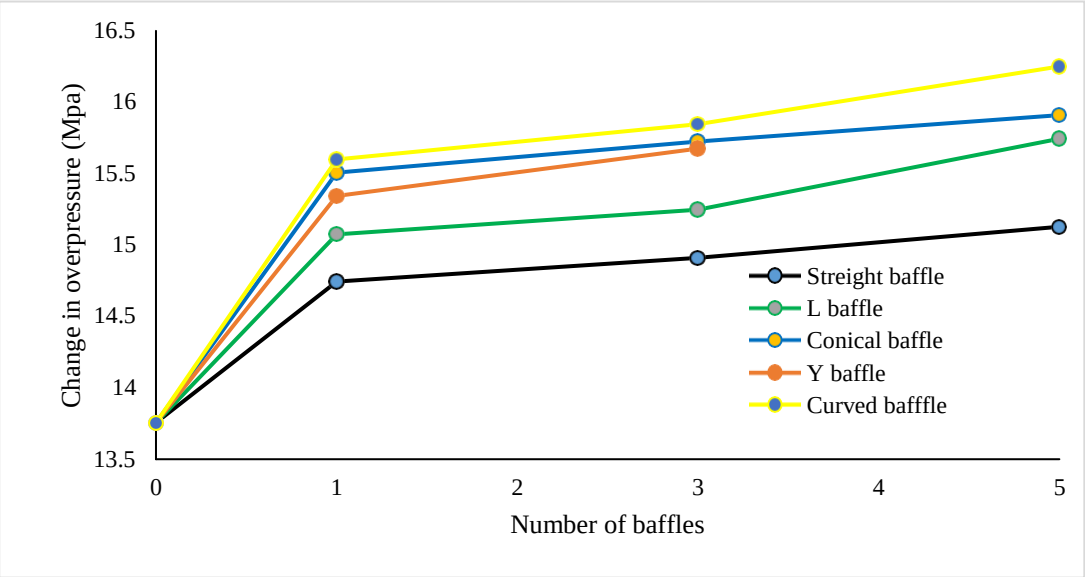

Figure 26. Change in overpressure vs. number of baffles

Change in pressure is the change between inlet pressure and maximum pressure at the exit of the suppressor. The change in overpressure value varies from baffle type to baffle type. And also, the chance of overpressure value increases when the number of baffles increases, as shown in Figure 26.

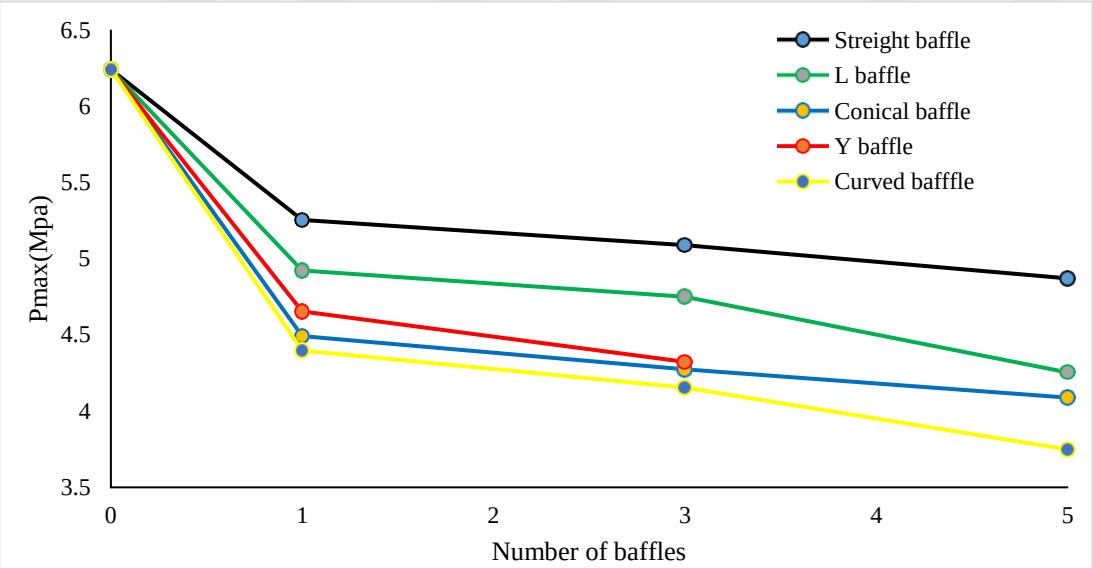

Figure 27. Maximum pressure vs. number of baffles

Maximum pressure is the pic pressure at the exit of the suppressor. In Figure 27, it is seen that the maximum pressure reduces when the number of baffles increases. It is also seen that suppressors with five curved baffles have lower maxim pressure.

5.3.2. Temperature

Temperature affects the density of the fluid, which affects the speed of sound. When the temperature lowers, the speed of the propellant gas lowers; this reduces the noise generated by the turbulent flow.

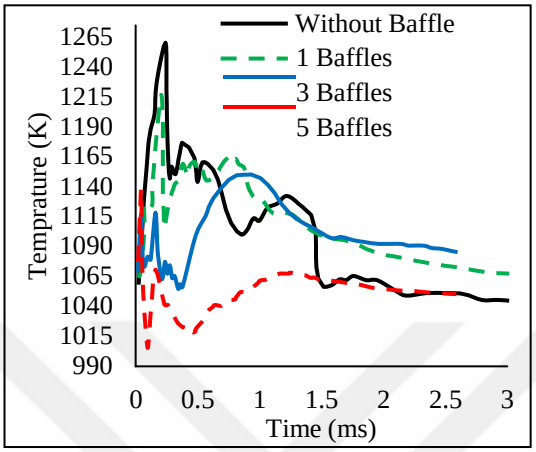

a. Straight baffle

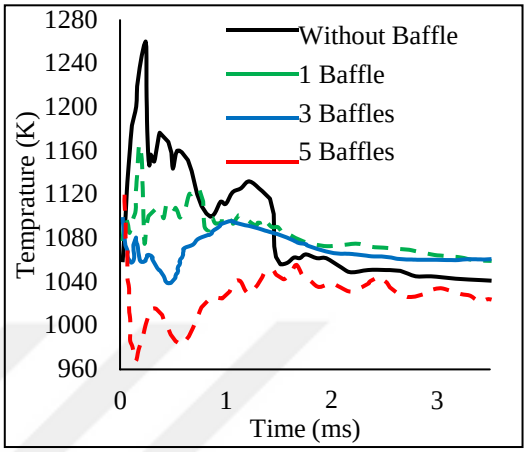

b. L baffle

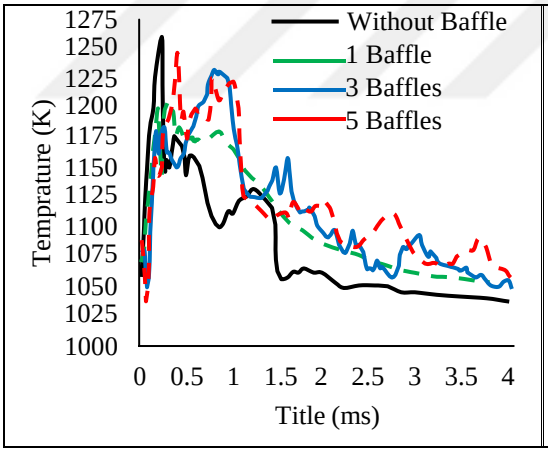

c. Conical baffle

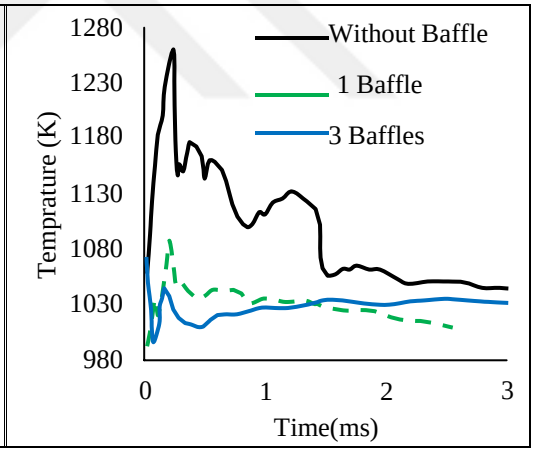

d. Y baffle

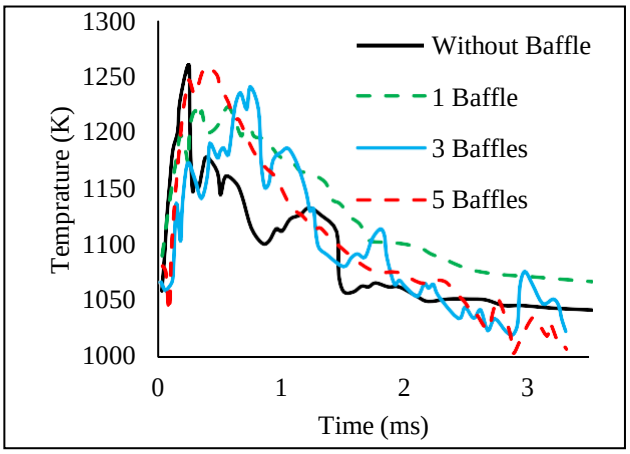

e. Curved baffle

Figure 28. Temperature vs. time graph of different types of suppressors

In this case, temperature reduction varies from 19.57% in the suppressor without a baffle to 28.44% in the suppressor with three Y baffles. As shown in Figure 28, in most cases, the temperature reduction increases when the baffling increases, but in some not; this is because of the decrease in internal volume. Increasing the baffles will reduce the internal volume, which is necessary for the gas to expand and lose its energy.

When the temperature decreases, the energy of the gas also decreases. This reduction in temperature has three main advantages. The first one lowers the formation of fire when the propellant gas mixes with the air. It also increases the attenuation of sound by avoiding the explosion. Lastly, it also increases the life of suppressor material.

5.3.3. Density

Density measures the amount of mass per unit of volume in a substance. The density and construction of the substance are directly proportional. The higher density of the gas has higher overpressure and carries high energy. This high density causes the formation of high sound amplitude. On the contrary, the decrease in density decreases both the overpressure and loudness of the explosion, so studying this parameter is also essential to understand the propellant flow further and design a good suppressor.

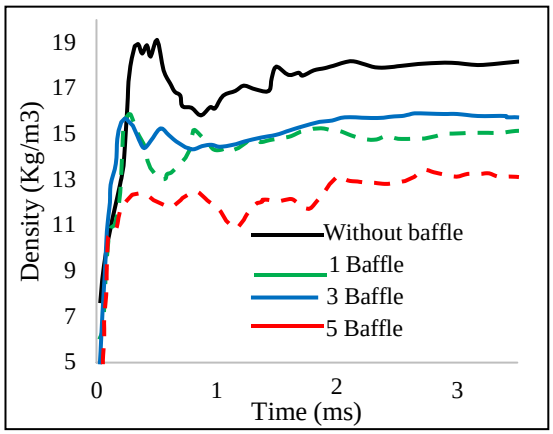

a. Straight baffle

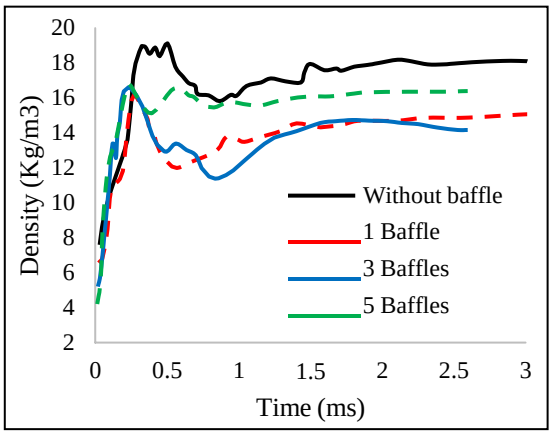

b. L baffle

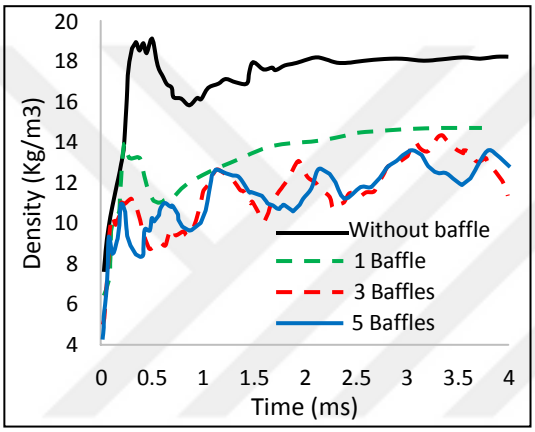

c. Conical baffle

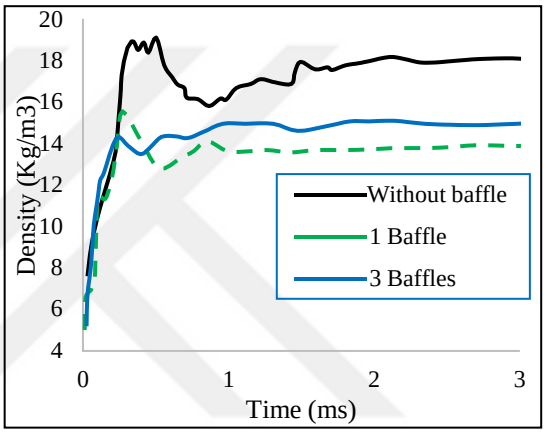

d. Y baffle

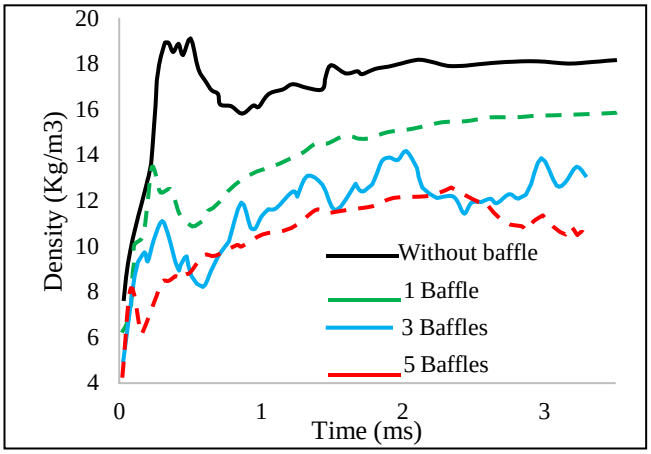

e. Curved baffle

Figure 29. Density vs. time graph of different suppressors

As seen in Figure 29, in most cases, maxim density occurred under 1ms, but when the number of baffles increased, the time to reach the pick also increased, and the pick

density value also reduced. The drop in pick density value affects the sound reduction positively. Compared to others, the pick density in suppressor with five curved baffles is very low.

5.3.4. Velocity

Velocity is also another essential factor that determines the effectiveness of the suppressor. In general, using the suppressor will increase the velocity of the suppressor, which is undesirable. But by using baffles in the side suppressor, it is possible to slow the rate of velocity increment.

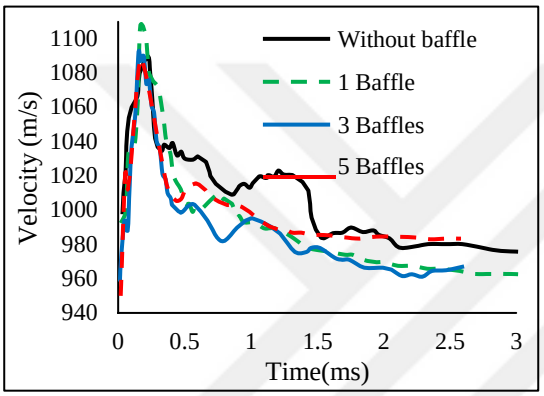

a. Straight

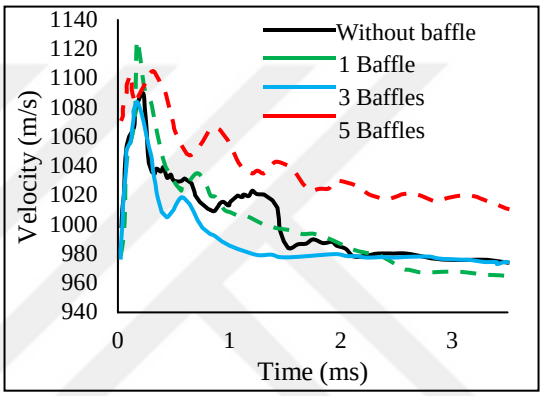

b. L baffle

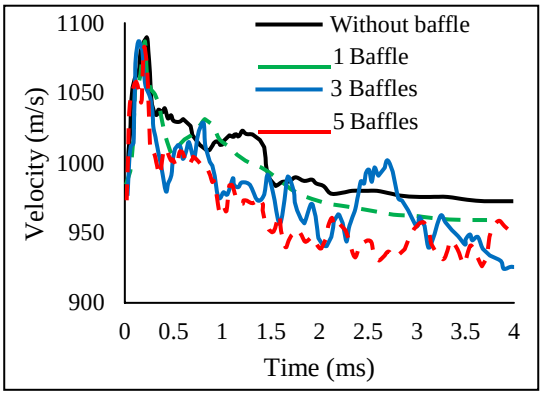

c. Conical baffles

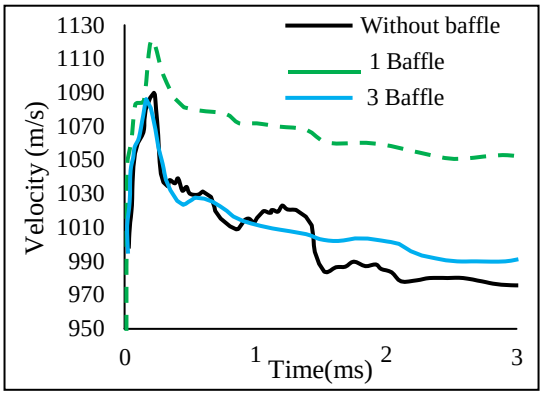

d. Y baffle

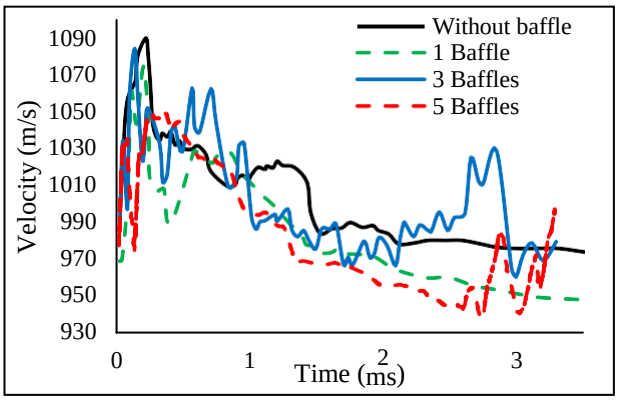

e. Curved baffle

Figure 30. Velocity Vs. Time graph of different suppressors

The study shows that increasing size increases the velocity but decreases the pressure. So, to correctly examine the performance of the suppressor, the calmative effect of velocity, pressure, and other fluid properties should be considered.

From figure 30, it is possible to say that increasing the number of baffles will increase obstacles that reduce velocity. Using a suppressor slows the motion of the fluid, but the extent of slowing depends on several factors, including the shape and size of mufflers and other fluid properties. In conclusion, using baffles in the side suppressor prevents explosion by avoiding the sudden release of gases into the surrounding.

Generally, studying all the above fluid parameters is necessary to understand the turbulence nature of the blast wave and to design the best suppressor. The overpressure is the most influencing parameter compared to other parameters. But all of these properties are related. When one changes, the other also varies directly or inversely proportional. Sound attenuation is the combined effect of all the above parameters and other conditions.

5.4. Different-sized suppressor with five curved baffles

5.4.1. Propellant flow analysis

In this section, the analysis of suppressors with five curved suppressors with increased diameter and length is presented. The investigation was done first by expanding the diameter by 1/6, keeping the other parameters constant. Second, the length of the suppressor was increased by 1/6 by keeping other conditions constant. Lastly, the analysis was done by increasing the diameter and length of the suppressor by 1/6. The results of all those conditions were compared to each other to investigate the effect of the volume of the suppressor on the effectiveness of suppressor sound attenuation. For the easiness of understanding, the models of the suppressor are represented by model numbers as follows:

- Model 1: Suppressor with zero baffles
- Model 2: Suppressor with one curved baffle
- Model 3: Suppressor with three curved baffles
- Model 4: Suppressor with five curved baffles
- Model 5: Increasing the diameter of the suppressor by 1/6, keeping the length and the number of baffles types constant
- Model 6: Increasing the length of the suppressor by 1/6, keeping the diameter and the number of baffles types constant
- Model 7: Increasing both the diameter and length of the suppressor by 1/6, keeping other parameters like time type and number of baffles constant

5.4.1.1. Pressure volume rendering

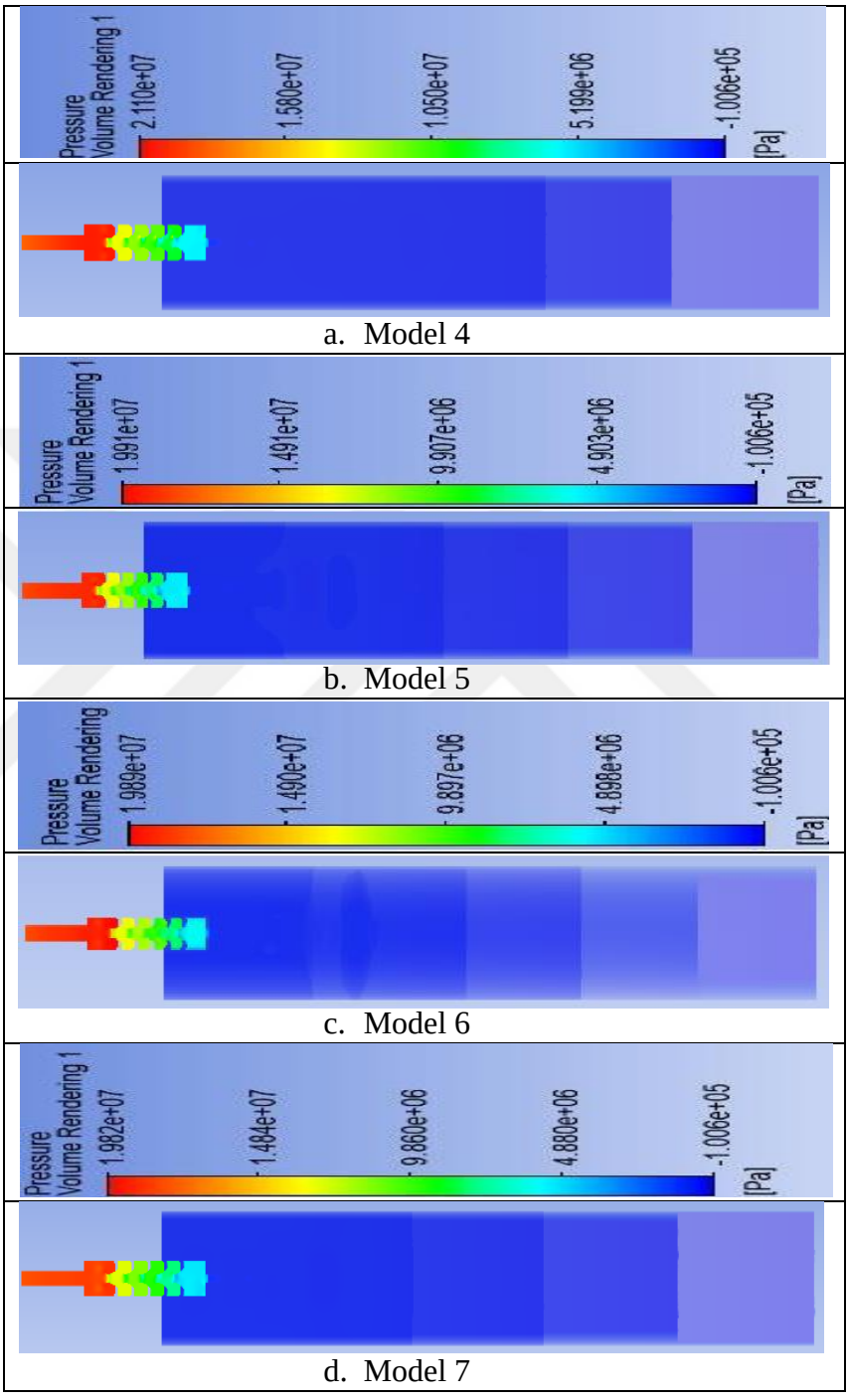

a. Model 4

b. Model 5

c. Model 6

d. Model 7

Figure 31. Pressure volume rendering of suppressor with five curved baffles

Figure The pressure-volume rendering figure shows that increasing the volume of the suppressor influences overpressure reduction. When the volume rises, the maximum overpressure reduces.

5.4.1.2. Velocity volume rendering

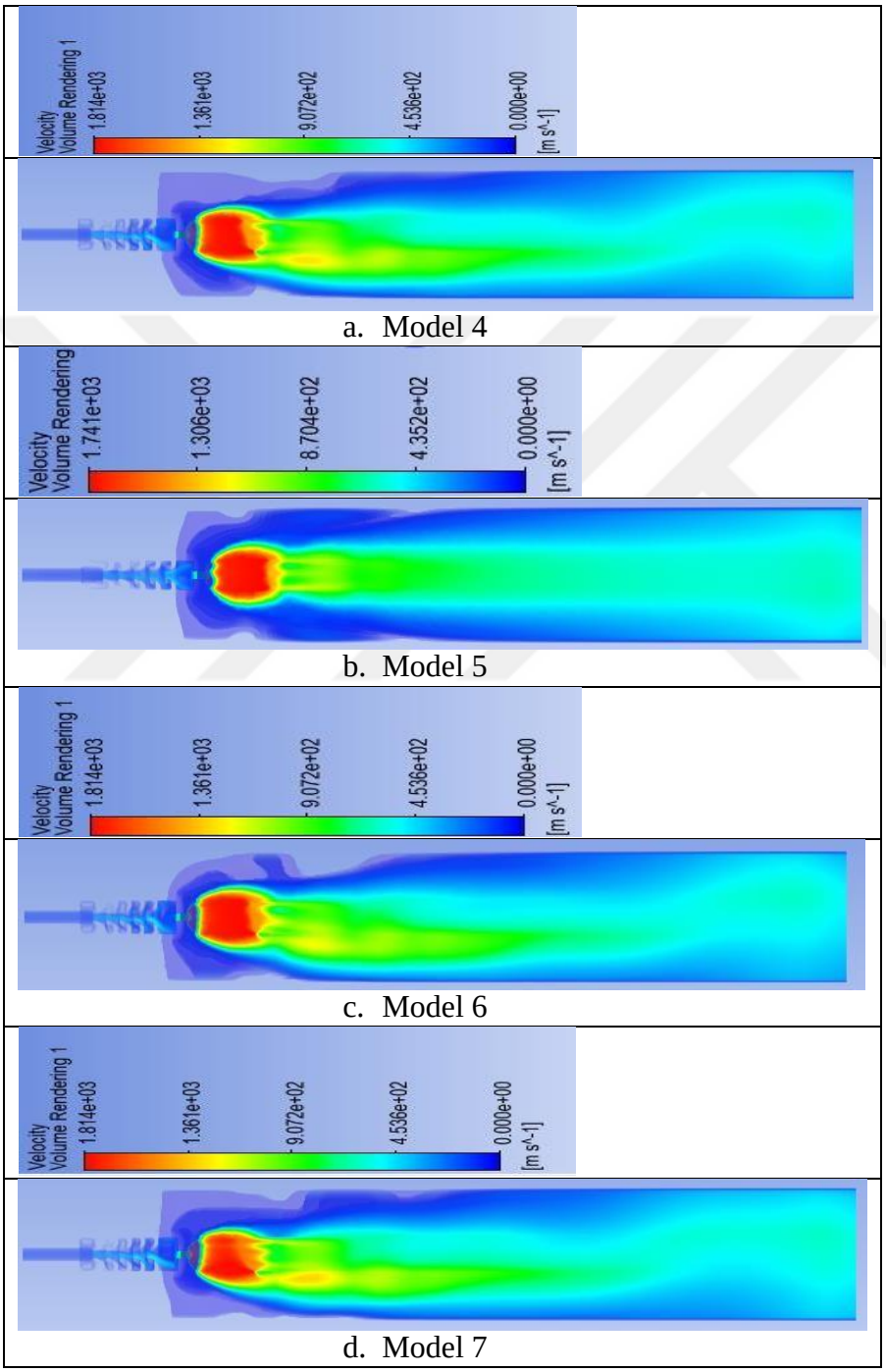

Figure 32. Velocity volume rendering of suppressor with five curved baffles

The velocity volume rendering figure shows that the fluid in front of the suppressor has a high velocity. From this, it can be concluded that propellant flow is directional. Figure 32 also shows that the velocity varies when the diameter and the length of the suppressor change.

5.4.1.3. Temperature volume rendering

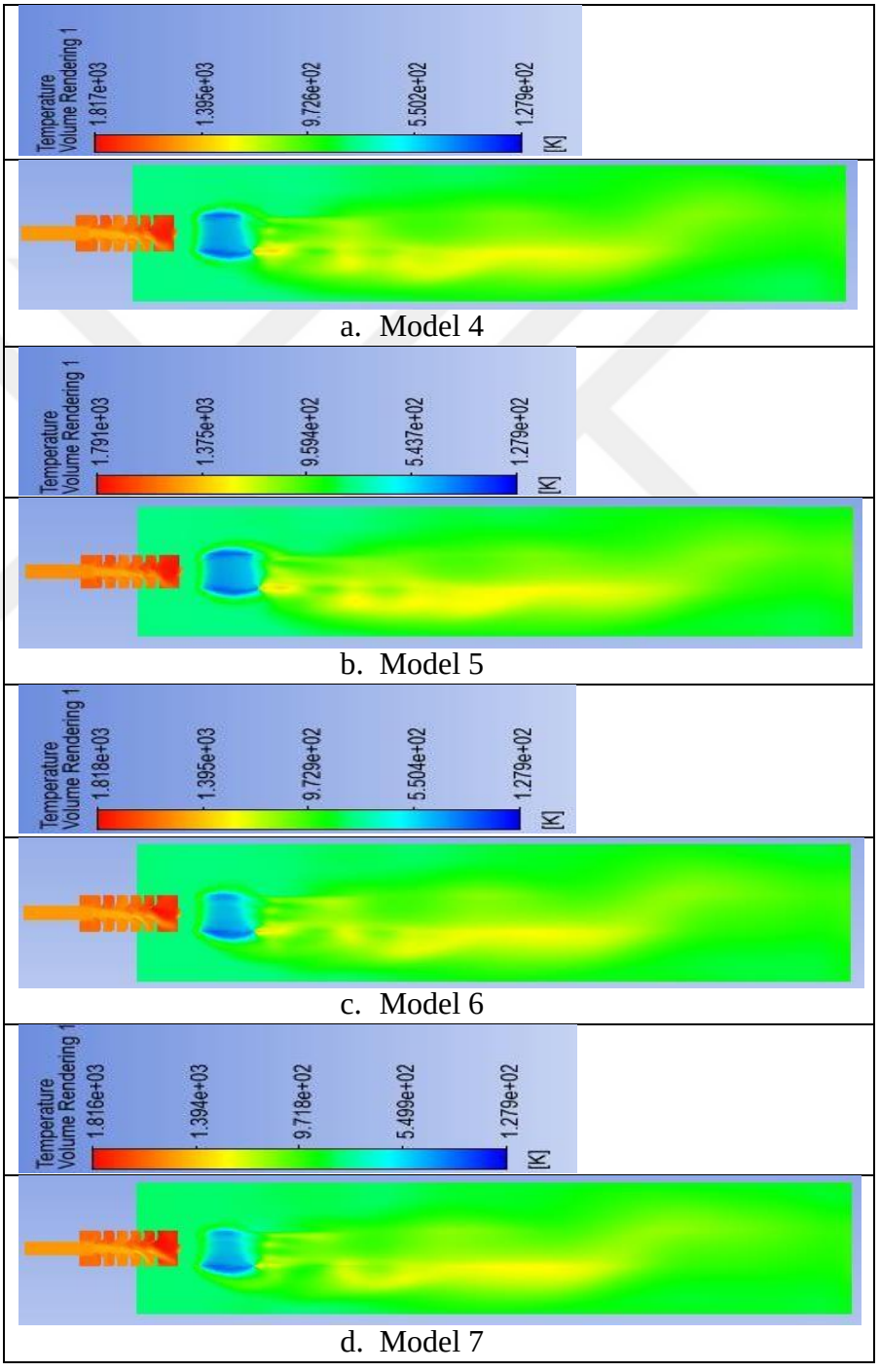

Figure 33. Temperature volume rendering of suppressors with five curved baffles

Figure 33 shows the temperature volume rendering inside and outside the suppressor. Like other volume renderings, the temperature rendering also shows a vibration when the volume of the suppressor varies.

5.4.2. Overpressure suppression analysis in a suppressor with five curved baffles

This section discusses the overpressure reduction result and the discussion of suppressors with five curved baffles.

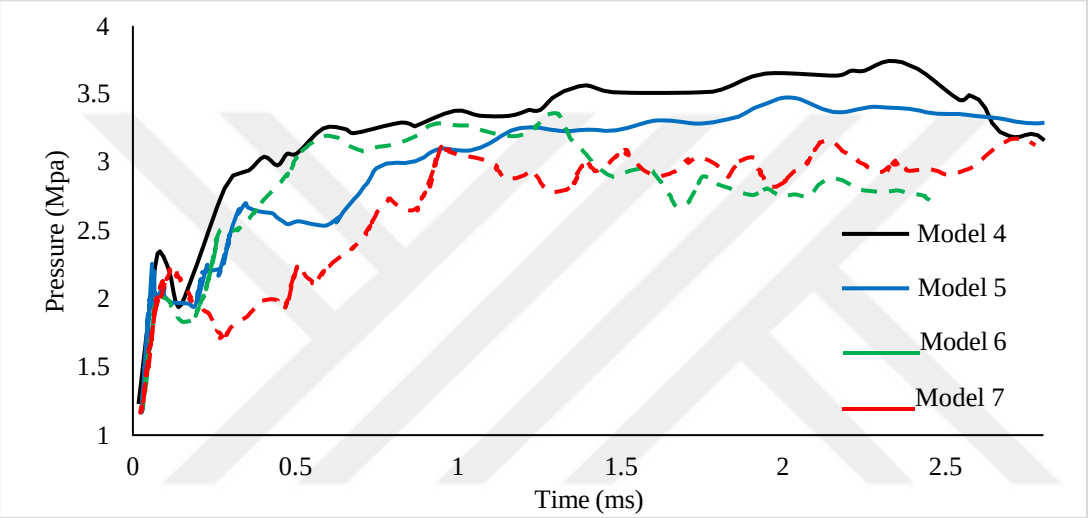

Figure 34. Pressure vs. time graph of suppressor with five curved baffles

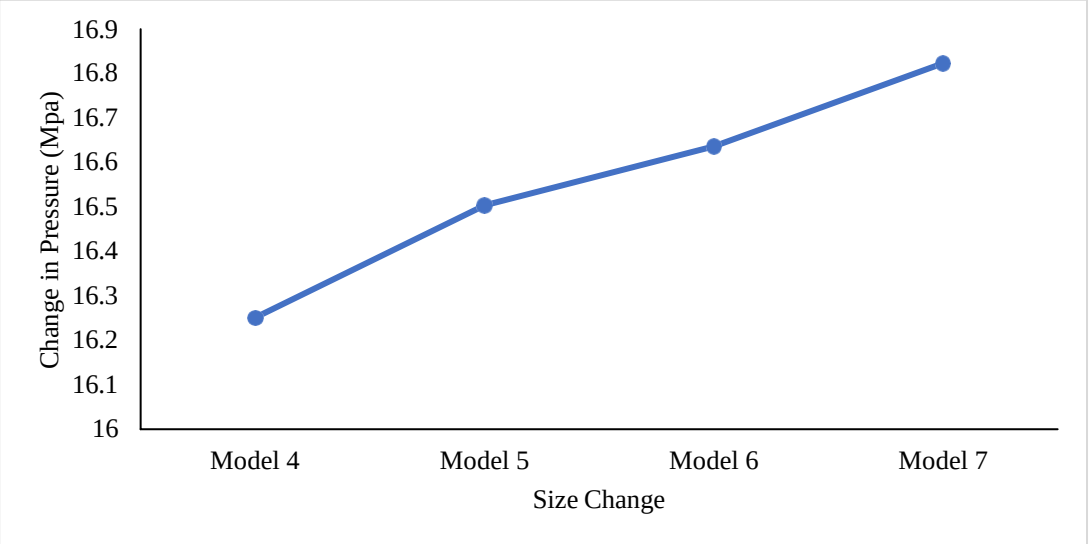

Figure 35. Pressure changes vs. size of suppressor

The overpressure reduction was 16.251 MPa when the suppressor was 20mm in diameter and 72mm in length. When the diameter was increased by one-sixth, the overpressure was reduced from 0.252Mpa to 16.503Mpa. When the length was increased by one-sixth, the overpressure decreased by 0.385Mpa to 16.636Mpa. Lastly, when the diameter and length of the suppressor increased by 1/6, the overpressure reduction increased by 0.57217066Mpa and became 16.82336653Mpa.

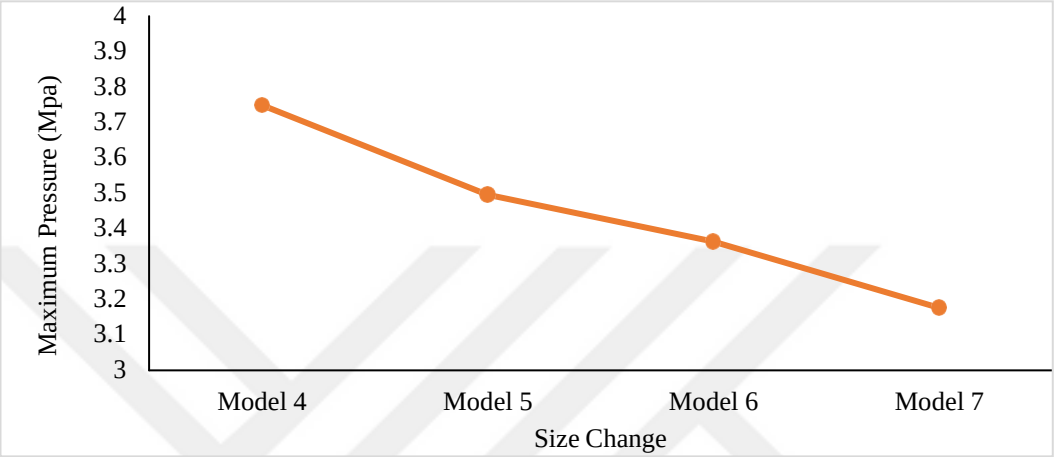

Figure 36. Maximum pressure vs. suppressor size

The maximum overpressure at model 4 was 3.748 MPa. However, when the diameter increased by 1/6, the maximum overpressure became 3.4961Mpa. When the suppressor's length increased by 1/6, the maximum overpressure became 3.3636Mpa. When the suppressor's diameter and length increased by 1/6, the maximum overpressure became 3.1766Mpa

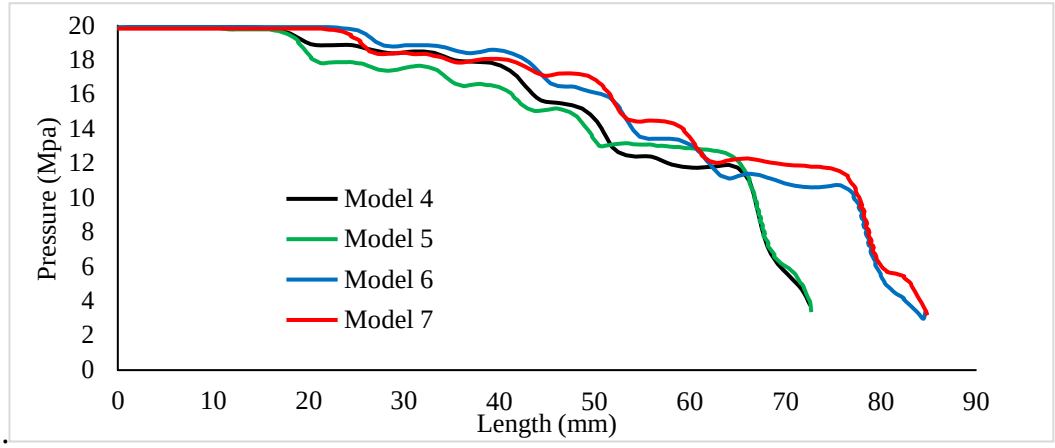

Figure 37. Pressure vs. length graph of suppressor with five curved baffles

The CFD analysis of the muzzle blast flow field generated by a small-caliber weapon during the blast flow is performed. The expansion volume of the Silencer is expanded before the muzzle to maximize attenuation. The first baffle, which receives the maximum pressure, reduces this maximum pressure and passes it on to the next baffle. As shown in Figure 37, there is an overpressure reduction inside the muffler.

5.4.3. Temperature reduction

Temperature is another critical factor that affects the performance of a suppressor. Reducing the temperature lowers the energy content of the gas, resulting in batter attenuation of sound. Figure 38 shows the temperature with five curved suppressors with different suppressor volumes.

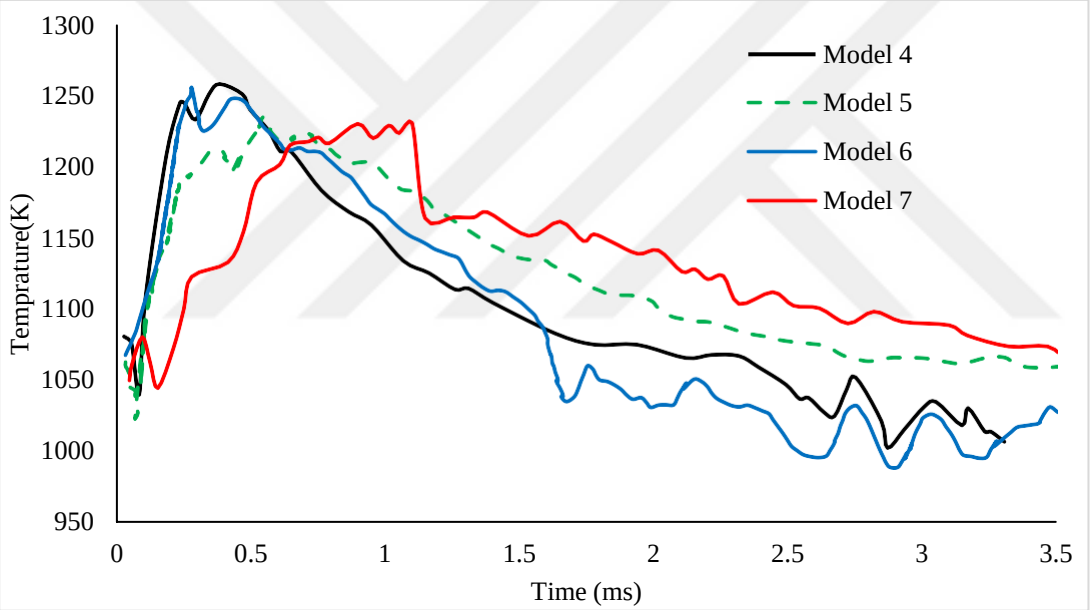

Figure 38. Temperature vs. time chart of suppressor with five curved baffle

As compared to the initial temperature, there is a reduction in temperature. And also, the maxim temperature of model 7 is lower. This result indicates that an increase in the volume of the suppressor decreases the temperature and increases the sound attenuation.

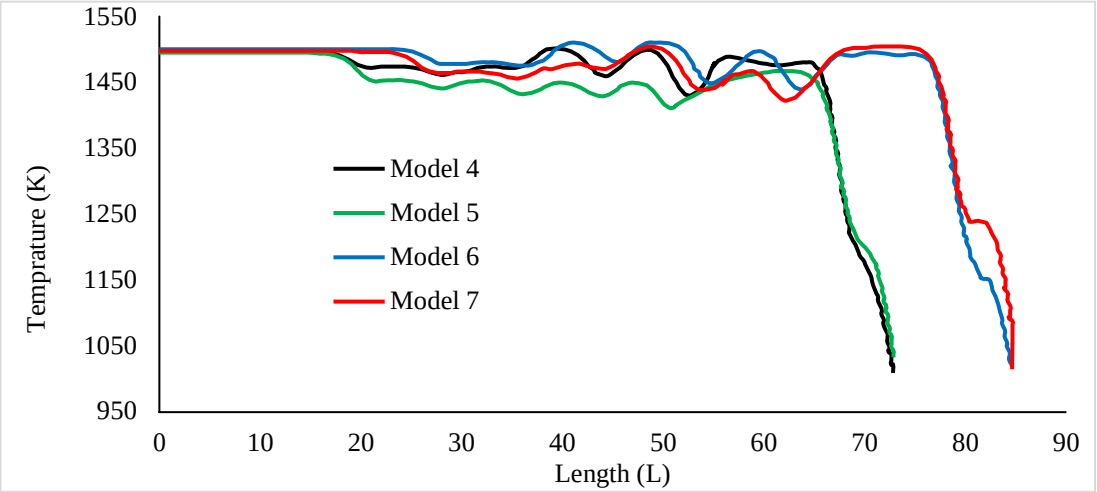

Figure 39. Temperature vs. length of suppressor for five curved suppressors

The effect of suppressor size, baffle number, and baffle shape on temperature reduction is shown in figure 38 and figure 39. The temperature reduction when both diameter and length increased by 1/6 becomes 484.86 K or 32.32%. The combined effect of temperature reduction and overpressure reduction gives maximum sound attenuation.

5.4.4. Velocity analysis and discussion

The velocity of the fluid creates turbulence and other waves inside and outside of the suppressor. The slow release of gunpowder gas into the ambient air lowers the tendency of explosion and increases sound attenuation.

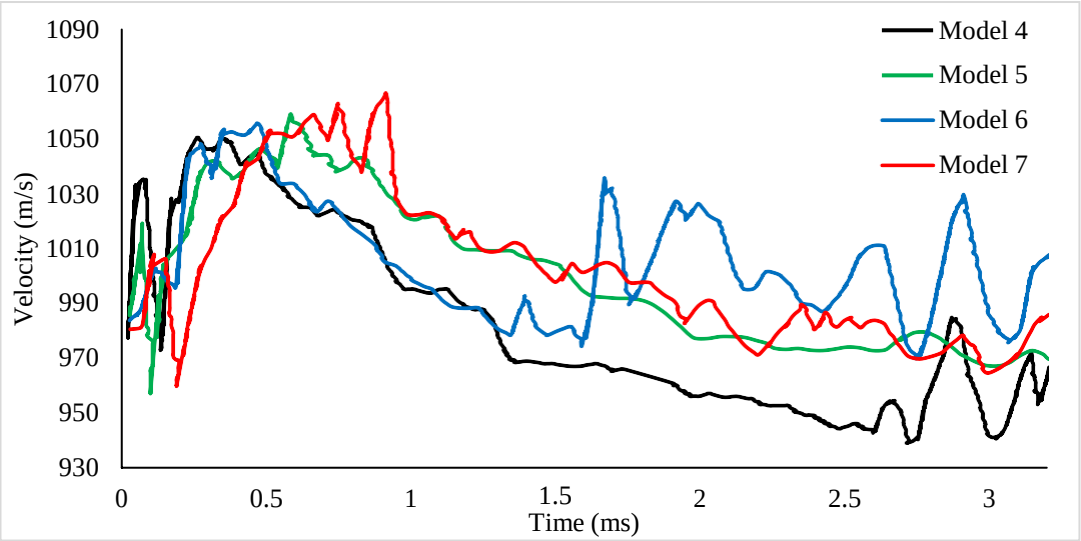

Figure 40. Velocity vs. time chart of suppressor with five curved baffle

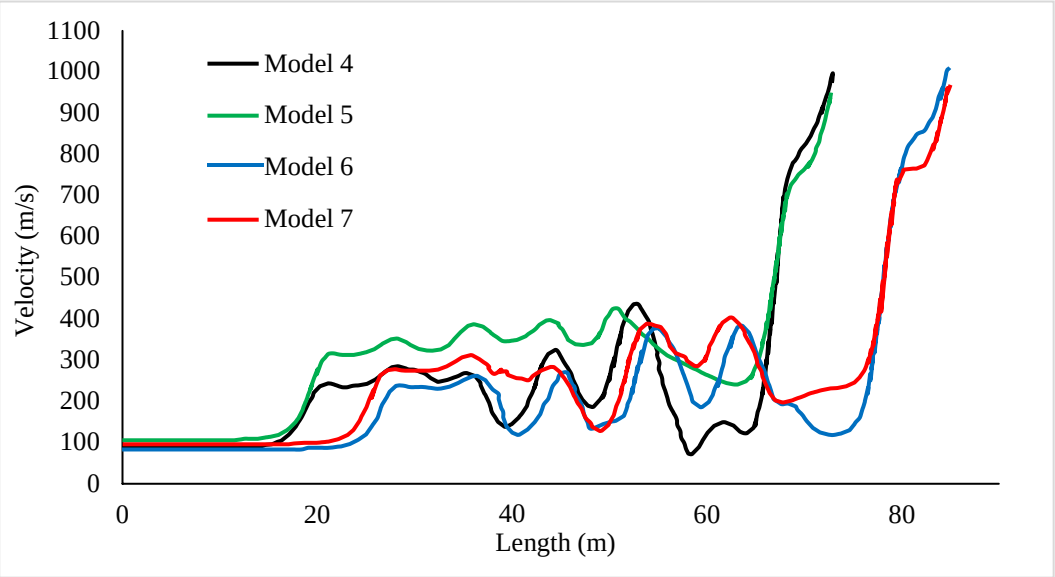

Figure 41. velocity vs. Length chart of suppressor with five curved baffles

5.4.5. Density results and discussion of suppressor with five curved baffles

Since density and pressure are directly related, lowering density gives better sound suppression by decreasing the overpressure of the gas. Density vs. time graphs for different cases is presented below.

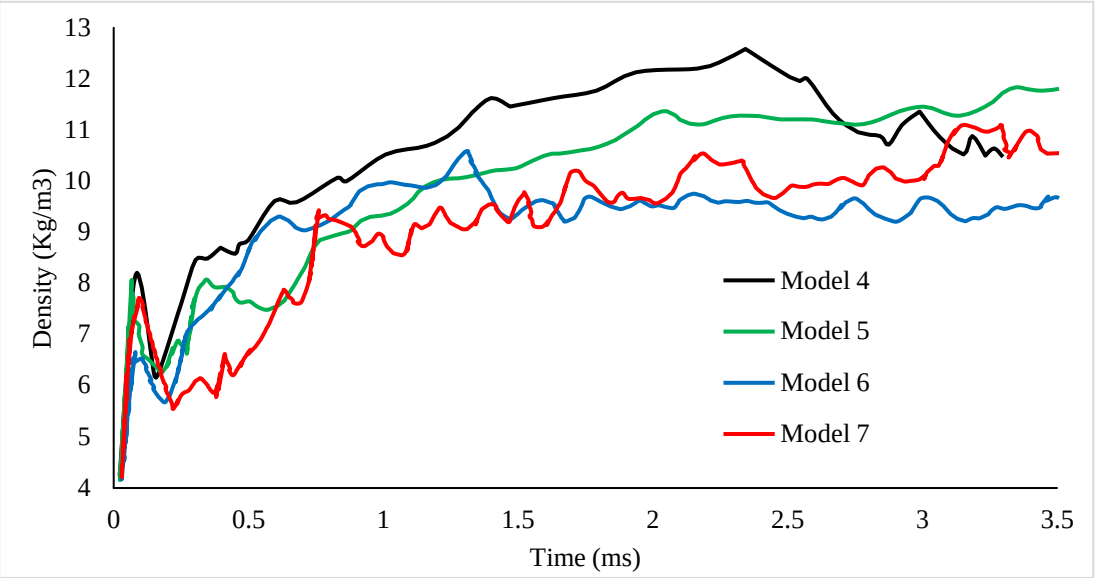

Figure 42. Density vs. time chart of suppressor with five curved baffle

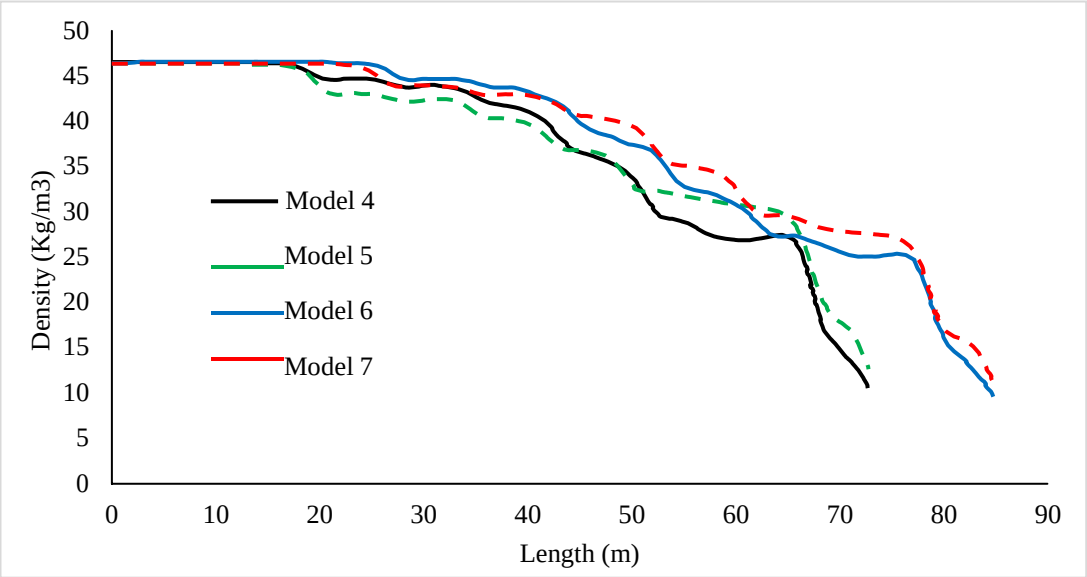

Figure 43. Density vs. length chart of suppressor with five curved baffles

5.5. Acoustic analysis suppressor with curved baffle

The sound pressure level, overall sound pressure level, and power spectral density were investigated to study the acoustic behavior. The receiver's location was 30 cm from the outlet of the Silencer.

5.5.1. Sound Pressure Level.

SPL peak is widely used as a global standard for weapon noise. The peak sound pressure level (SPL peak) and OASPL were estimated by simulating the turbulent gas flow. This study used Ffowcs Williams and Hawking's acoustics models to calculate the far-field sound signals. The fast Fourier transform FFT was also used to post-process the acoustic pressure signals.

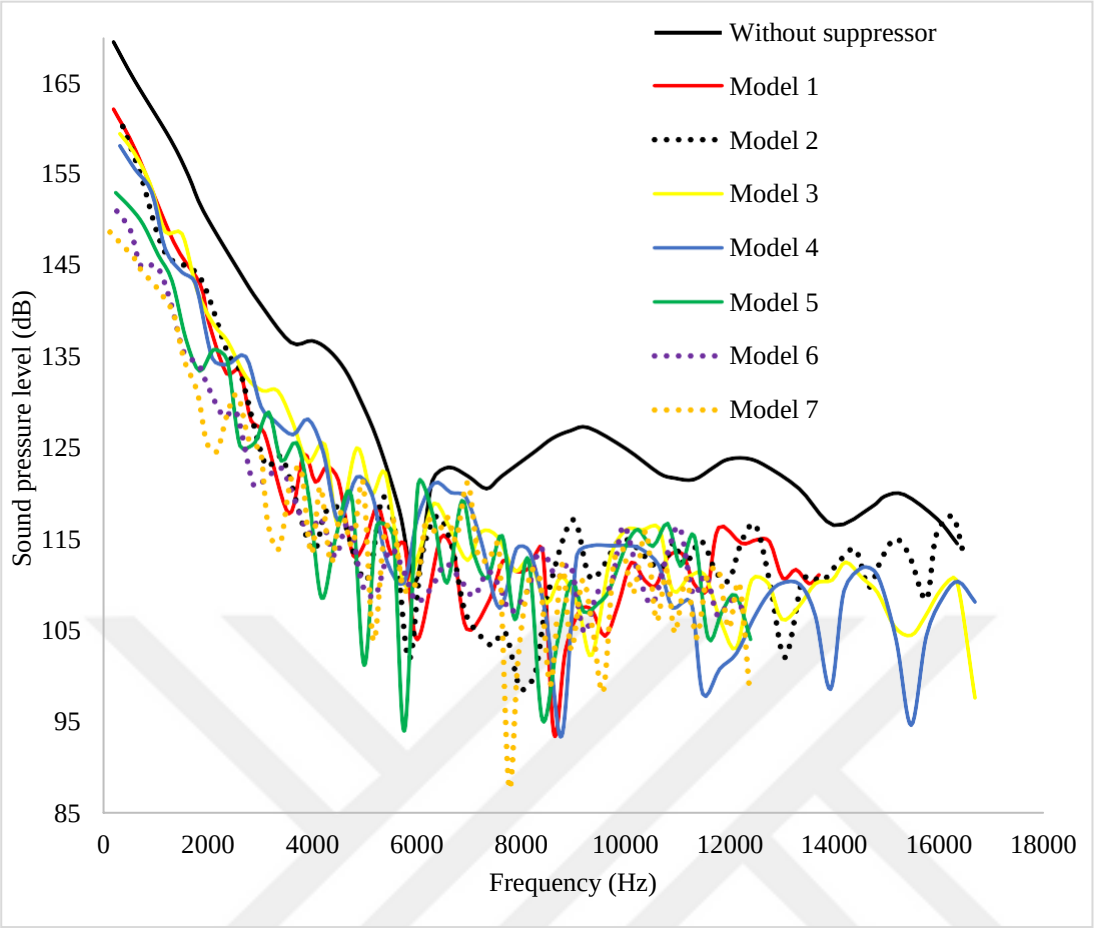

Figure 44. Sound pressure level vs. frequency chart of suppressor with curved baffles

The numerical analysis of propellant gas from the gun without a suppressor recorded 169.498 dB of sound pressure level. When using a suppressor without a baffle, 7.745 dB of SPL attenuation was achieved and became 162.134 dB. The SPL was reduced by 7.745 dB for a suppressor with one curved and became 160.234 dB. When the baffling number increased to three, the sound pressure level attenuation increased to 10.594 dB and became 159.437 dB. The SPL value for a suppressor with five curved baffles was 158.117 dB or 11.381 dB attenuation. For a suppressor with five curved baffles, when the diameter increased by 1/6, the SPL attenuation increased to 16.515 dB, which became 152.983 dB. When the length increased by 1/6, the attenuation was 17.541 dB, and the sound pressure value became 150.956 dB. Lastly, when the suppressor diameter and length increased by 1/6, the sound pressure attenuation increased by 20.835 dB and became 148.663 dB.

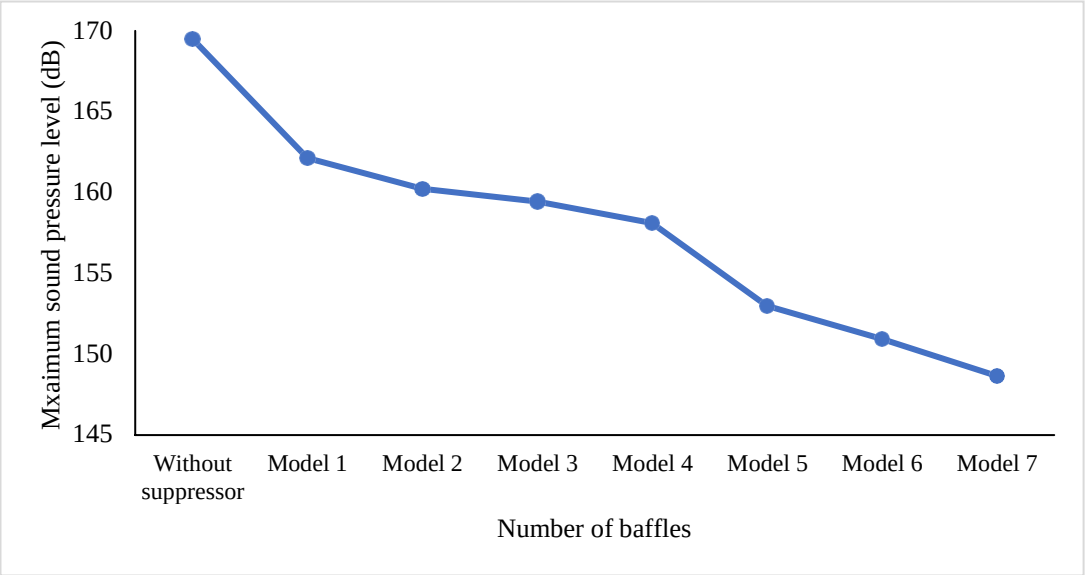

Figure 45. Maximum sound pressure level vs. number of baffles for curved suppressor

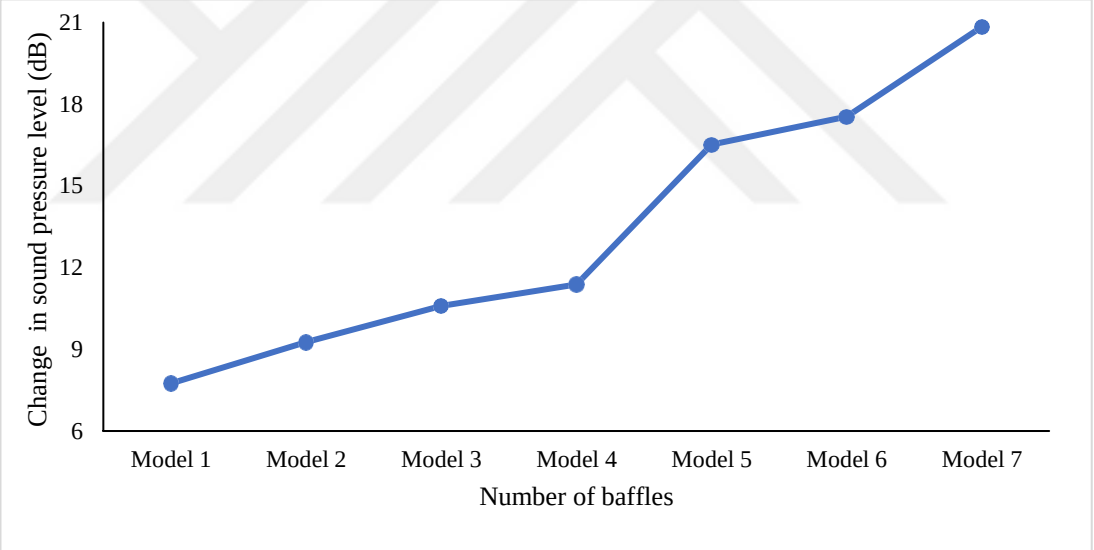

Figure 46. Change in sound pressure level vs. number of baffles for curved suppressor

A peak SPL value was decreased from 169.498 dB in an unsuppressed condition to 148.663 dB. Figure 46 shows a 20.835 dB or 12.29 % reduction of peak SPL using a curved suppressor.

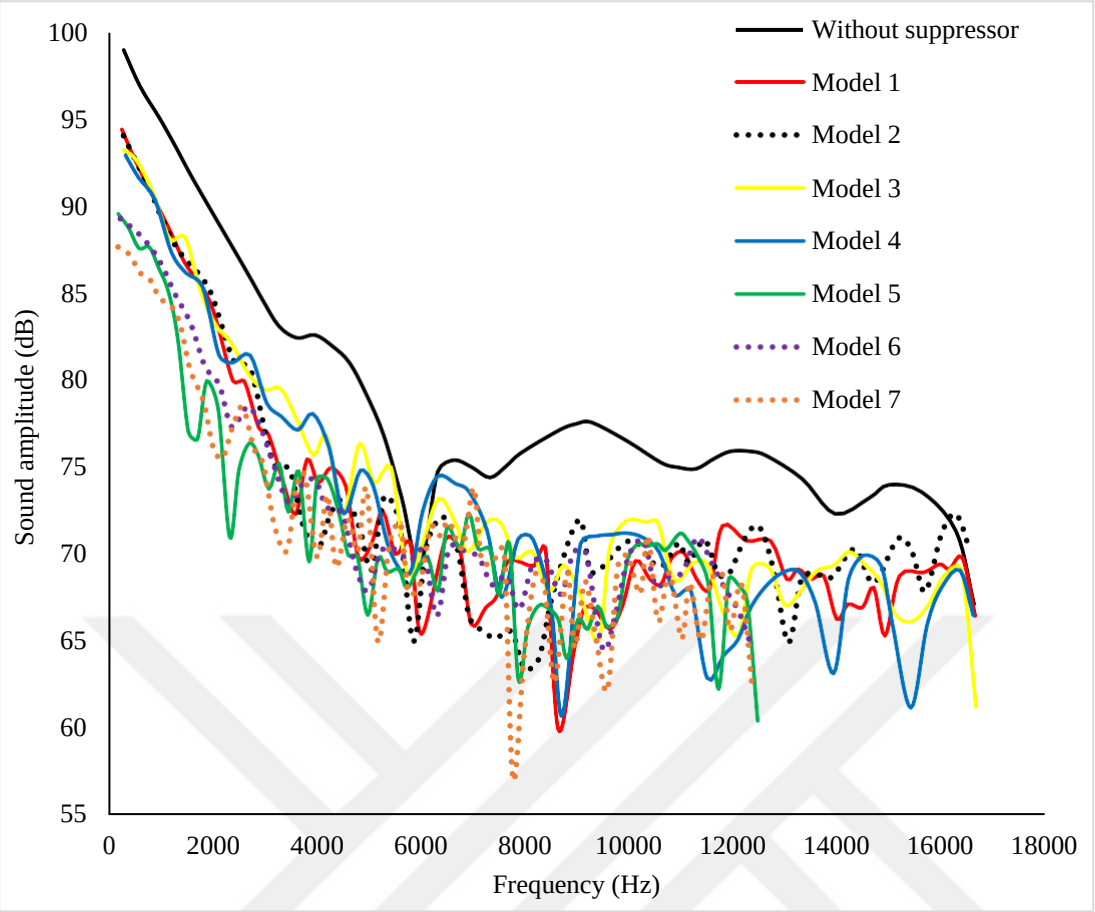

Figure 47. Sound amplitude vs. frequency chart of suppressor with curved baffles

The sound amplitude without a suppressor was 98.995 dB. This value decreased to 94.424dB (4.570dB sound amplitude attenuation) for the suppressor without a baffle. The attenuation of a suppressor with one curved baffle increased to 4.936 dB and became 94.058 dB. When the baffling number increased to thee, the attenuation also increased to 5.754 dB and became 93.241 dB. In addition, when the baffles were increased to five, the attenuation rose to 6.059 dB, and the sound amplitude became 92.936 dB. For the suppressor with five curved baffles, when the diameter was increased by 1/6, the attenuation was raised to 9.435dB. In addition, when the length was increased by 1/6, the sound amplitude raised to 9.714dB. Lastly, when both diameter and length were increased by 1/6, the attenuation increased to 11.345 dB and became 87.649dB.

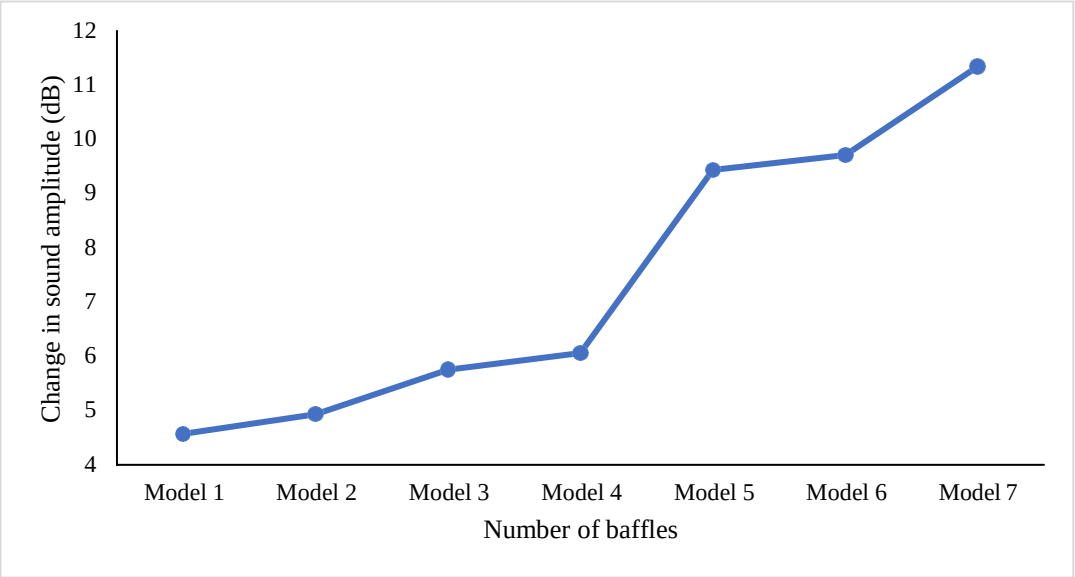

Figure 48. Change in sound amplitude Vs. Number of the baffle of suppressor with curved baffle

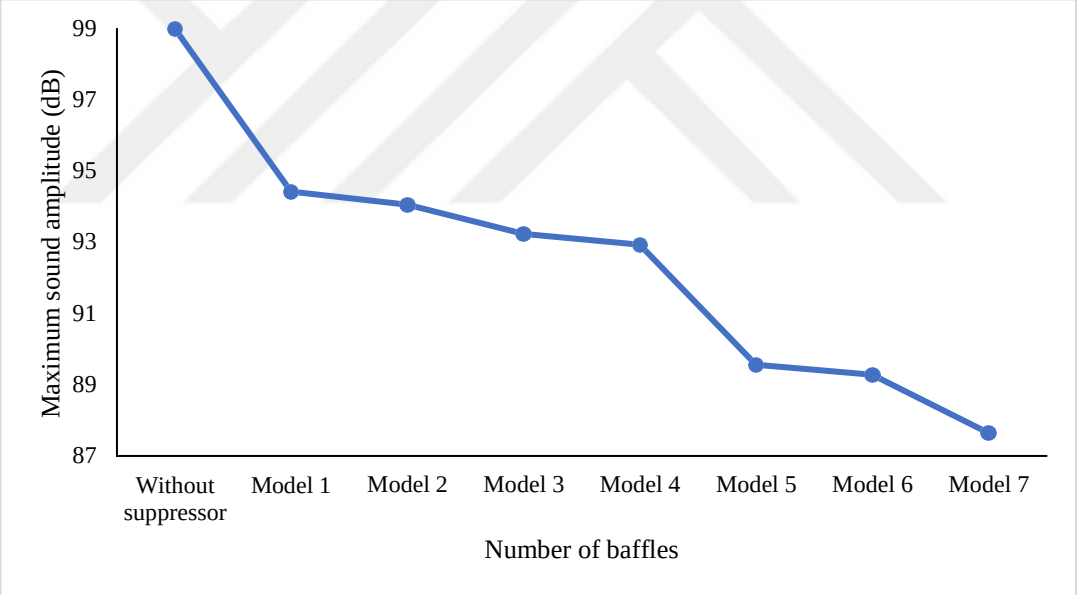

Figure 49. Maximum sound amplitude vs. number of baffles of suppressor with curved baffle

The maximum sound amplitude decreased from 98.16 dB to 87.64dB. The muffler predicted attenuation of nearly 11.34 dB

5.2.2. Power spectral density (PSD)

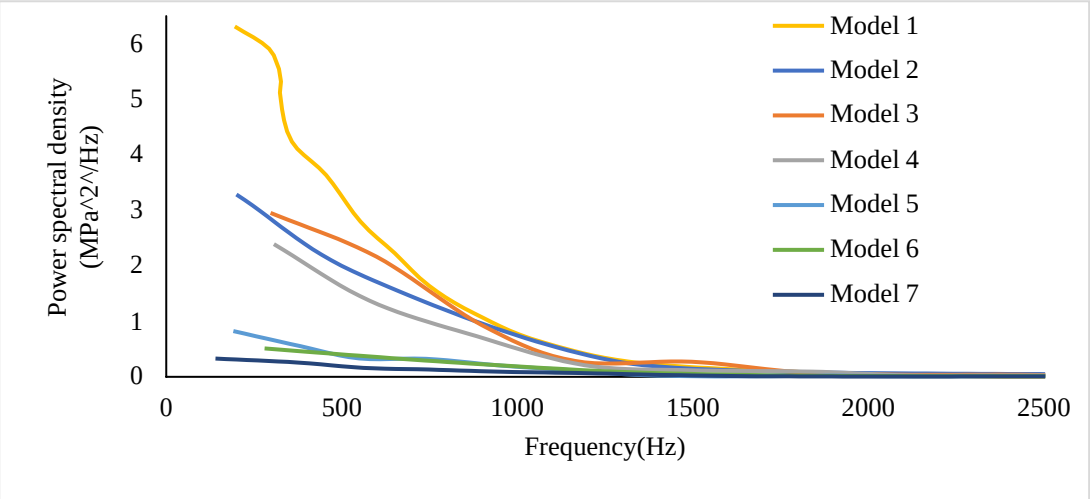

Figure 50. Sound spectral density vs. frequency of suppressor with curved baffle

As shown in Figure 50, the power spectral density decreased from model 1 (suppressor without baffle) to model 7 (suppressor with five curved, and both width and dimension were extended by1/6). According to this graph, increasing the number of baffles and the volume of the suppressor (diameter and length) decreases the explosion's power spectral density (SPD). When SPD drops, the loudness decreases, resulting in better attenuation.

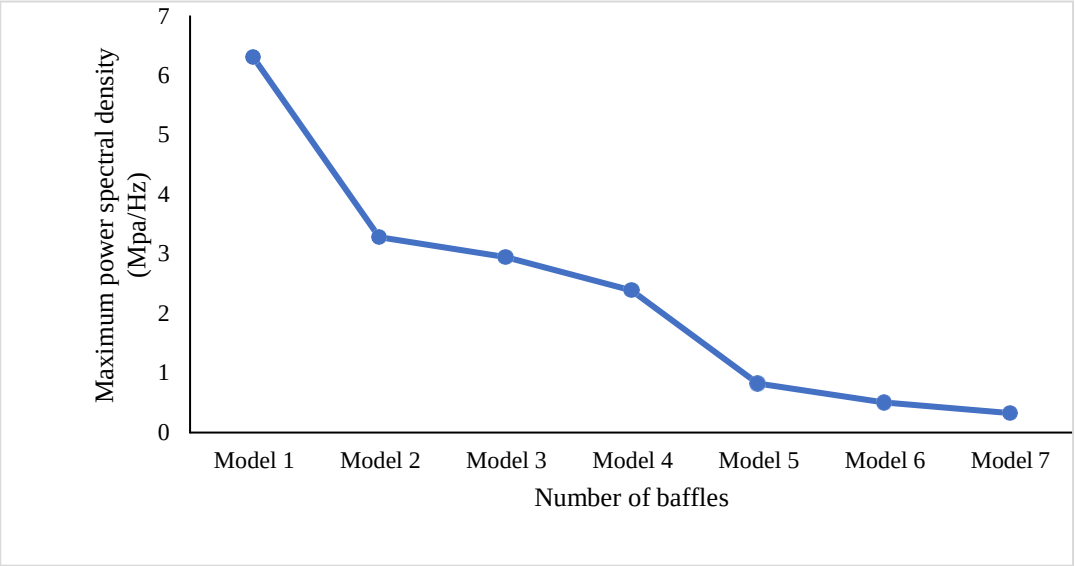

Figure 51. Maximum sound spectral density vs. number of baffle chart of suppressor with curved baffle

The maximum power spectral density without a suppressor was 35 Mpa^2/Hz). With this SPD, the power levels in each frequency component are very high; this results in a loud noise. Using a suppressor reduces this SPD level and gives a better attenuation. For a suppressor without a baffle, the maximum sound spectral density value decreased from 35 Mpa^2/Hz to 6.313 Mpa^2/Hz, which is 28.686 Mpa^2/Hz. When one curved baffle was used in a suppressor, the maximum sound spectral density value was reduced to 3.283 Mpa^2/Hz.

When the baffling number was further increased to 3 and 5, the maximum sound spectral density value was reduced to 2.952 Mpa^2/Hz and 2.389 Mpa^2/Hz, respectively. Increasing the suppressor volume also further reduces the SPD value. For the suppressor with five curved baffles, when the diameter was increased by one-six, the length increased by one-six, and both diameter and length increased by one-six, the value of SPD was reduced to 0.823 Mpa^2/Hz, 0.51Mpa^2/Hz and 0.327 Mpa^2/Hz respectively.

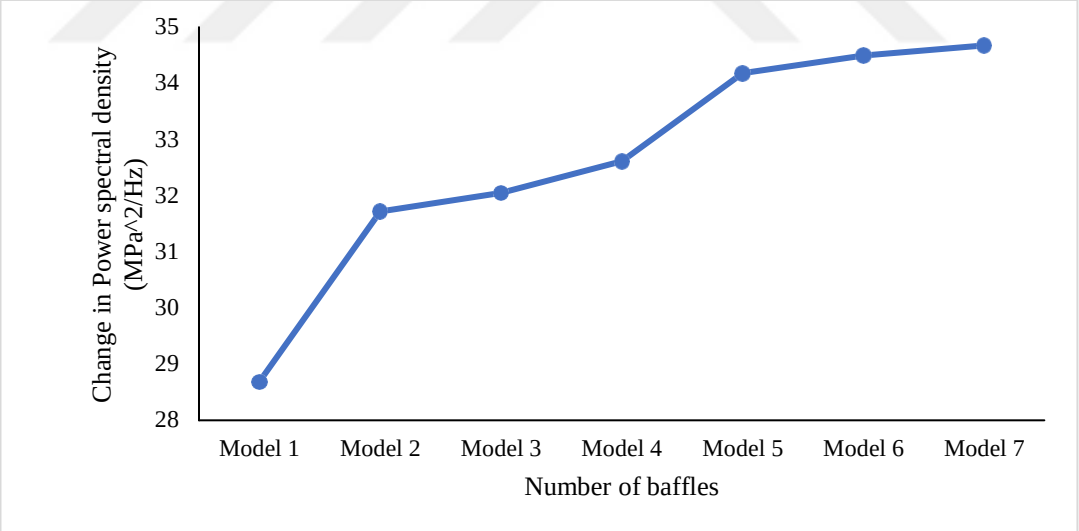

Figure 52: Change in sound spectral density vs. number of baffle charts of suppressor with the curved suppressor

From the Figure, it is clear that there is a significant reduction in power spectral density, this reduction in PSD results in better attenuation. The simulations show that such a design reduces the amount of overpressure and acoustic noise.

6. CONCLUSIONS

A better understanding of the various processes during the firing cycle was achieved in the numerical simulation. In particular, the suppressor reveals the turbulent flow, vortices' formation, and gas flow in the expansion chambers. The suppressor's efficiency seems to be that the propellant gasses are released more slowly, reducing the pressure wave and giving the combustible mixture more time to react with the ambient oxygen and cool down fully. From this point of view, the suppressor's efficiency is directly proportional to its size, shape of baffles, and ability to generate as many eddy currents as possible to act as a capacitor with a slower release of the accumulated energy. This study used CFD and CAA methods to simulate the fluid and impulse noise.

This study used a CFD-CAA hybrid method to simulate the impulse noise of a rifle with and without a suppressor. The model was validated by comparison with experimental data. In this study, the maximum attenuation was achieved in a suppressor with five curved baffles when the diameter and length increased by one-six. This suppressor achieved a 20.835 dB sound pressure level attenuation with 16.823 MPa overpressure reduction and 484.86 K or 32.32% temperature reduction.

The conclusions can be summarized as follows: The attenuation of the Silencer generally increases with its internal volume. The increase in diameter and length of the suppressor increases the attenuation. But for excellent design, a proper balance between suppressor size and attenuation is necessary to reduce the adverse effect of suppressor weight and size. Attenuation also increases when the number of the baffle is more. Another factor that increases the noise reduction is the complexity of the baffle inside the suppressor, and complex geometries have a better suppression. Lastly, this paper recommends using more complex geometries, and wire mashes to reduce the gas's energy content. This way, more batter attenuation can get. This study also suggests using large-eddy simulations (LES) and chemical reactions of gunpowder gases, if possible, which will help to get precise results.

REFERENCES

Aimée Lister. (2006). Investigations into the Optimisation of Sound Suppressor Geometry. *Ph.D.Thesis*. URI:http://hdl.handle.net/1826/1629.

Alam, M. F. (2013). A dynamic hybrid RANS/LES modeling methodology for turbulent/transitional flow field prediction. *Thesis (Ph.D.)--Mississippi State University;* Publication Number: AAT 3603414; ISBN: 9781303580161;

Alkan, B., & Atayılmaz, S. O. (2018). A HYBRID NUMERICAL/EXPERIMENTAL STUDY OF THE AERODYNAMIC NOISE PREDICTION. In *Journal of Thermal Engineering* (Vol. 4, Issue 4). Yildiz Technical University Press.

ANSYS. (2022). Ansys® Academic Research fluent, Release 2022 R1, Help System, *Theory guide, Aerodynamically Generated Noise, ANSYS, Inc.*

Araya, G. (2019). Turbulence model assessment in compressible flows around complex geometries with unstructured grids. *Fluids*, *4*(2). https://doi.org/10.3390/fluids4020081.

Arslan, H., Ranjbar, M., Secgin, E., & Celik, V. (2020). Theoretical and experimental investigation of acoustic performance of multi-chamber reactive silencers. *Applied Acoustics*, *157*. https://doi.org/10.1016/j.apacoust.2019.07.035.

Blake, J. D., Sescu, A., Thompson, D., & Hattori, Y. (2022). A Coupled LES-Synthetic Turbulence Method for Jet Noise Prediction. Aerospace, 9(3), 171. https://doi.org/10.3390/AEROSPACE9030171

Bozdemir, M., Üniversitesi, K., Savunma Teknolojileri Bölümü, F., & Tarihi, G. (2019). Havalı Silah Sistemleri İçin Tek Parçalı Susturucu Tasarımı * Single Particle Suppressor Design For Airgun Systems Antalya, *Türkiye'de sempozyumda sunulmuştur*. *18*. https://doi.org/10.17134/khosbd.561195.

Cler, D. L., Chevaugeon, N., Shephard, M. S., Flaherty, J. E., & Remacle, J.-F. (2003). *CFD Application to Gun Muzzle Blast-A Validation Case Study Two CFD codes, Fluent 6.1.11 (a pre-release version of Fluent)*.

Crighton, D. G. (1977). Aeroacoustics. By Marvin E. GOLDSTEIN. McGraw-Hill, 1976. *Journal of Fluid Mechanics*, https://doi.org/10.1017/S0022112077211256.

Deardorff, J. W. (1970). A numerical study of three-dimensional turbulent channel flow at large Reynolds numbers. *Journal of Fluid Mechanics*, https://doi.org/10.1017/S0022112070000691.

Dempster, J. (2001). Signal Analysis and Measurement. *The Laboratory Computer*, https://doi.org/10.1016/B978-012209551-1/50039-8.

Garnier, E., Adams, N., & Sagaut, P. (2009). Large Eddy Simulation for Compressible Flows. https://doi.org/10.1007/978-90-481-2819-8

Elsayed, N. M., & Gorbunov, N. v. (2007). Pulmonary Biochemical and Histological Alterations after Repeated Low-Level Blast Overpressure Exposures. *Toxicological Sciences*, *95*(1), 289–296. https://doi.org/10.1093/TOXSCI/KFL138.

Ffowcs Williams, J. E., & Hawkings, D. L. (1969). Sound generation by turbulence and surfaces in arbitrary motion. *Roy Soc London-Philosophical Trans Ser A*, *264*(1151), 321–342. https://doi.org/10.1098/RSTA.1969.0031.

Foltz, A. L. (2019). *Experimental and numerical analysis of small caliber gun barrels under internal pressure fatigue loading*.

Gong, Y. (2012b). Large Eddy Simulation of dispersed multiphase flow. Dissertations, Master's Theses, and Master's Reports - Open. https://doi.org/10.37099/mtu.dc.etds/729

Guo, Z., Pan, Y., Li, K., & Zhang, H. (2013). Numerical simulation of overpressure about muzzle blast flowfield. *Advanced Materials Research*, *605–607*, 2506–2509. https://doi.org/10.4028/www.scientific.net/AMR.605-607.2506.

Hanafi, A., & Khlifi, H. (2016). Evaluation study of pressure-strain correlation models in compressible flow. *Journal of Applied Fluid Mechanics*, *9*(6), 2685–2693. https://doi.org/10.29252/jafm.09.06.25601.

Hodor, V., Birle, D., Nascutiu, L., & Deac, I. (2017). Aeroacoustics - Noise Prediction by Using "LES" for Signal Processing. *Energy Procedia*, *112*, 322–329. https://doi.org/10.1016/j.egypro.2017.03.1104.

Hristov, N., Kari, A., Jerkovi, D., Savić, S., & Sirovatka, R. (2015). Simulation and Measurements of Small Arms Blast Wave Overpressure in the Process of Designing a Silencer. *Measurement Science Review*, *15*(1), 27–34. https://doi.org/10.1515/msr-2015-0005.

Hristov, N., Kari, A., Jerković, D., & Savić, S. (2018). Application of a CFD model in the determination of the muzzle blast overpressure in small arms and its validation by measurement. *Tehnicki Vjesnik*, *25*(5), 1399–1407. https://doi.org/10.17559/TV-20180321135212.

Hudson, M. K., Luchini, C., Keith, J., & Shyy, W. (2001). *The Evaluation of Computational Fluid Dynamics Methods for the Design of Muzzle Blast Suppressors for Firearms*.

Huerta-Torres, J. K., Silva-Rivera, U. S., Verduzco-Cedeño, V. F., Flores-Herrera, L. A., & Sandoval-Pineda, J. M. (2021). Numerical and experimental analysis of sound suppressor for a 5.56 mm caliber. *Defense Science Journal*, *71*(1), 12–17. https://doi.org/10.14429/DSJ.71.14957.

JAMES E., & CASKEY, JR. (1963). *GENERAL CIRCULATION EXPERIMENTS WITH THE PRIMITIVE EQUATIONS*. Monthly Weather Review Volume 91 Issue 3. https://doi.org/https://doi.org/10.1175/1520-0493(1963)091<0099:GCEWTP>2.3.CO;2.

Jean DASSÉ. (2006). *CERFACS CFD-Combustion Sous la direction de Bénédicte cuenot simulation numérique directe de la combustion turbulente avec ntmix3d*.

Kang, K. J., Ko, S. H., & Lee, D. S. (2008). A study on impulsive sound attenuation for a high-pressure blast flowfield. *Journal of Mechanical Science and Technology*, *22*(1), 190–200. https://doi.org/10.1007/s12206-007-1023-8.

Keith Hudson, M., Luchinh, C., Keith Clutter, J., & Shyys, W. (1996). CFD approach to firearms sounds suppressor design. *32nd Joint Propulsion Conference and Exhibit*, 1–12. https://doi.org/10.2514/6.1996-3020.

Kim, H. (2012). *The transmission loss of silencers with flow from a flow-impedance tube*.

Klingenberg, G., & Mach, H. (1976). Investigation of Combustion Phenomena Associated with the Flow of Hot Propellant Gases I: Spectroscopic Temperature Measurements Inside the Muzzle Flash of a Rifle. In *COMBUSTION AND FLAME* (Vol. 27).

Le Roy, T. W. (2011). *Muffler characterization with the implementation of the finite element method and experimental techniques*. https://doi.org/10.37099/mtu.dc.etds/381.

Lee, H. S., Kang, T. Y., & Hong, J. H. (2018). Development of a Muffler for 40 mm Medium Caliber Gun: Numerical Analysis and Validation. *International Journal of Precision Engineering and Manufacturing*, *19*(2), 245–250. https://doi.org/10.1007/s12541-018-0028-9.

Li, P. Fei, & Zhang, X. bing. (2021). Numerical research on the adverse effect of muzzle flow formed by muzzle brake considering secondary combustion. *Defence Technology*, *17*(4), 1178–1189. https://doi.org/10.1016/j.dt.2020.06.019.

Lo, S. W., Tai, C. H., & Teng, J. T. (2011). Axial-symmetry numerical approaches for noise predicting and attenuating of rifle shooting with suppressors. *Journal of Applied Mathematics, 2011*. https://doi.org/10.1155/2011/961457.

Maccarthy, M., O'neill, M., & Cripps, H. (2011). An investigation into the use of sound moderators on firearms. *For game and feral management in new south wales for game and wild management in New South Wales*. https://ro.ecu.edu.au/ecuworks2011/858.

Matyushenko, A. A., & Garbaruk, A. v. (2016). Adjustment of the k-ω SST turbulence model for prediction of airfoil characteristics near stall. *Journal of Physics: Conference Series*, *769*(1), 012082. https://doi.org/10.1088/1742-6596/769/1/012082.

Menter, F. R. (1994). Two-equation eddy-viscosity turbulence models for engineering applications. *AIAA Journal*, *32*(8), 1598–1605. https://doi.org/10.2514/3.12149.

Miller, S. L., & Childers, D. (2004). Power Spectral Density. *Probability and Random Processes*, 369–411. https://doi.org/10.1016/B978-012172651-5/50010-5.

Murphy, W. J., Flamme, G. A., Campbell, A. R., Zechmann, E. L., Tasko, S. M., Lankford, J. E., Meinke, D. K., Finan, D. S., & Stewart, M. (2018). The reduction of gunshot noise and auditory risk through the use of firearm suppressors and low-velocity ammunition. *International Journal of Audiology*, *57*, S28–S41. https://doi.org/10.1080/14992027.2017.1407459.

ÖZBEKTAŞ, S., & SUNGUR, B. (2021). Mermi Hareketinin Modellenmesinde Kullanılan Noble-Abel ve İdeal Gaz Denklemlerinin Akış Alanına Etkisinin Nümerik İncelenmesi. *European Journal of Science and Technology*. https://doi.org/10.31590/EJOSAT.1012916.

Paeres, D., Lagares, C., & Araya, G. (2022). Assessment of Turbulence Models over a Curved Hill Flow with Passive Scalar Transport. *Energies 2022, Vol. 15, Page 6013*, *15*(16), 6013. https://doi.org/10.3390/EN15166013.

Per Rasmussen, Michael Stewart, Greg Flamme, Deanna Meinke, & James Lankford. (n.d.). *Measuring Recreational Firearm Noise*. www.SandV.com.

Pitsch, H., Pitsch, & Heinz. (2006). Large-Eddy Simulation of Turbulent Combustion. *AnRFM*, *38*(1), 453–482. https://doi.org/10.1146/ANNUREV.FLUID.38.050304.092133.

Rehman, H., Chung, H., Joung, T., Suwono, A., & Jeong, H. (2011). CFD analysis of sound pressure in tank gun muzzle silencer. *J. Cent. South Univ. Technol*, *18*. https://doi.org/10.1007/s11771−011−0936−7.

Seçgin, E., Arslan, H., & Birgören, B. (2021). A statistical design optimization study of a multi-chamber reactive type silencer using simplex centroid mixture design. *Journal of Low-Frequency Noise Vibration and Active Control*, *40*(1), 623–638. https://doi.org/10.1177/1461348419901227.

Selech, J., Kilikevičius, A., Kilikevičiene, K., Borodinas, S., Matijošius, J., Vainorius, D., Marcinkiewicz, J., & Staszak, Z. (2020). Force and sound pressure sensors used for modeling the impact of the firearm with a suppressor. *Applied Sciences (Switzerland)*, *10*(3). https://doi.org/10.3390/app10030961.

Silencer (firearms) - Wikipedia. (n.d.). Retrieved August 27, 2022, from https://en.wikipedia.org/wiki/Silencer_(firearms)

Smith, J. D., Adams, B. R., Jackson, R., Smith, Z., Suo-Antilla, A., Smith, S., & Allen, D. (2017). *RANS vs. LES CFD for Gas-Fired Combustion Equipment Analysis*.

SST k-omega model -- CFD-Wiki, the free CFD reference. (n.d.). Retrieved August 19, 2022, from https://www.cfd-online.com/Wiki/SST_k-omega_model.

Sullivan, P. P., McWilliams, J. C., & Moeng, C. H. (1994). A subgrid-scale model for large-eddy simulation of planetary boundary-layer flows. *Boundary-Layer Meteorology 1994 71:3*, *71*(3), 247–276. https://doi.org/10.1007/BF00713741.

Sun, G., & Domaradzki, J. A. (2018). Implicit LES using adaptive filtering. *Journal of Computational Physics*, *359*, 380–408. https://doi.org/10.1016/J.JCP.2018.01.009.

The Science of Sound. (n.d.). Retrieved December 20, 2021, from https://www.nasa.gov/specials/X59/science-of-sound.html

Tushar Chindha, J., & Sanjay Bhaskar, Z. (2015). Performance evaluation of reactive Silencer. *International Engineering Research Journal*, *2*, 5696–5699. www.ierjournal.org.

Uruba, V. (2019). Reynolds number in laminar flows and turbulence. *AIP Conference Proceedings*, *2118*. https://doi.org/10.1063/1.5114728.

Wagner, C., Hüttl, T., & Sagaut, P. (2007). Large-Eddy Simulation for Acoustics. *Large-Eddy Simulation for Acoustics*, *9780521871440*,1–441. https://doi.org/10.1017/CBO9780511546143.

White, M. (1998). The use of sound suppressors on high-powered rifles. *Small Arms Review*, *1*(7–9). http://guns.connect.fi/gow/highpow.html.

Xu, X., Battaglia, F., Chaudhuri, S., Colver, G. M., Rajagopalan, G. R., & Tannehill, J. C. (2003). *Large eddy simulation of compressible turbulent pipe flow with heat transfer*.

Yucetepe, M., Molki, M., Darabi, J., & Yan, T. (2015). *Liquid-Gas Recirculation and Entrainment in a Wall-Driven Cavity*.

Zhang, H., Chen, Z., Jiang, X., & Li, H. (2013). Investigations on the exterior flow field and the efficiency of the muzzle brake. *Journal of Mechanical Science and Technology*, *27*(1), 95–101. https://doi.org/10.1007/s12206-012-1223-8.

Zhao, X. Y., Zhou, K. D., He, L., Lu, Y., Wang, J., & Zheng, Q. (2019). Numerical Simulation and Experiment on Impulse Noise in a Small Caliber Rifle with Muzzle Brake. *Shock and Vibration*, *2019*. https://doi.org/10.1155/2019/5938034.

Zhipeng Lou. (2017). Improved flamelet modeling of supersonic combustion. *Journal of Propulsion and Power*. doi:10.2514/1.b36779.

RESUME

Name Surname: Ezedin Ayaliew YIMAM

Date of Birth:

Foreign Language: English and Turkish

Education Level:

Bachelor's: Jimma University, Mechanical engineering 2017

Master's Degree: Kırıkkale University, Mechanical engineering 2022

Research Areas: Energy and Fluid dynamics